

# Electrospun Chitosan-Based Nanofibrous Coating for the Local and Sustained Release of Vancomycin

Stefano Serpelloni, Michael Ellis Williams, Sergio Caserta, Shashank Sharma, Maham Rahimi, and Francesca Taraballi\*



Cite This: *ACS Omega* 2024, 9, 11701–11717



Read Online

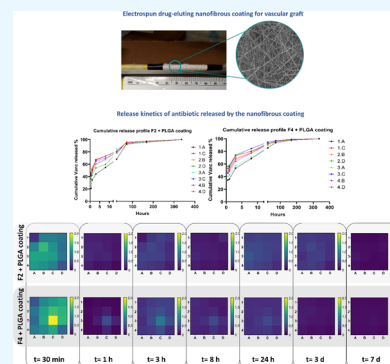
ACCESS |

Metrics & More

Article Recommendations

Supporting Information

**ABSTRACT:** As the population ages, the number of vascular surgery procedures performed increases. Older adults often have multiple comorbidities, such as diabetes and hypertension, that increase the risk of complications from vascular surgery including vascular graft infection (VGI). VGI is a serious complication with significant morbidity, mortality, and healthcare costs. Here, we aimed to develop a nanofibrous chitosan-based coating for vascular grafts loaded with different concentrations of the vancomycin antibiotic vancomycin (VAN). Blending chitosan with poly(vinyl alcohol) or poly(ethylene oxide) copolymers improved solubility and ease of spinning. Thermal gravimetric analysis and Fourier transform infrared spectroscopy confirmed the presence of VAN in the nanofibrous membranes. Kinetics of VAN release from the nanofibrous mats were evaluated using high-performance liquid chromatography, showing a burst followed by sustained release over 24 h. To achieve longer sustained release, a poly(lactic-co-glycolic acid) coating was applied, resulting in extended release of up to 7 days. Biocompatibility assessment using human umbilical vein endothelial cells demonstrated successful attachment and viability of the nanofiber patches. Our study provides insights into the development of a drug delivery system for vascular grafts aimed at preventing infection during implantation, highlighting the potential of electrospinning as a promising technique in the field of vascular surgery.



## INTRODUCTION

In recent decades, there has been an increase in vascular surgery procedures, which is largely attributed to the aging population. A recent UN study predicts that by 2030, the number of people over 65 will double, leading to a corresponding increase in the incidence of vascular diseases.<sup>1–3</sup> Aging is associated with a number of changes in the cardiovascular system, including increased arterial stiffness and decreased vascular compliance, which can result in hypertension and other cardiovascular diseases.<sup>4,5</sup> Localized changes in the arterial wall may lead to atherosclerosis and peripheral arterial disease (PAD), associated with severe claudication, rest pain, and major limb loss.<sup>6,7</sup> Treating symptomatic PAD often requires vascular grafts. Vascular surgery in older adults can present unique challenges<sup>7,8</sup> due to the presence of multiple comorbidities such as congestive heart failure, hyperlipidemia, chronic kidney disease, diabetes, and hypertension, increasing the risk of postsurgery complications, including vascular graft infection (VGI).<sup>9–11</sup> VGI is a serious and potentially life-threatening complication,<sup>12</sup> posing complex and multifaceted challenges that can result in significant morbidity, mortality, and healthcare costs.<sup>13,14</sup> These infections can be caused by a variety of microorganisms, including bacteria and fungi, and can result in a range of clinical manifestations, from local wound infections to systemic infections with sepsis and multiorgan failure.<sup>15,16</sup> The

incidence of VGI varies depending on several factors, including the type of graft, location of graft, urgency of operation, patient comorbidities, and surgical technique used. The reported incidence of VGI is estimated to be between 1 and 6%,<sup>17,18</sup> with higher rates reported in patients with certain comorbidities. Intraoperative contamination is considered the most common cause of graft infections, closely followed by infection from nearby sites. Implications of VGI cannot be understated, with affected patients suffering mortality rates as high as 70%.<sup>19,20</sup> Prevention and treatment of VGI have proven to be a great challenge, and there are no ideal prosthetic conduits. Despite advances in surgical techniques and antimicrobial therapies, the VGI remains a major challenge for clinicians and researchers. Novel strategies for preventing and treating VGI are needed, and scientists have started to explore different solutions such as the development of new antimicrobial agents,<sup>21–23</sup> the use of biomimetic designs for graft material,<sup>21,24–27</sup> and the use of gene therapy to enhance the immune response to infection or guide vascular regeneration.<sup>27–30</sup>

**Received:** November 15, 2023

**Revised:** February 7, 2024

**Accepted:** February 13, 2024

**Published:** February 28, 2024



**Table 1. Composition and Properties of the Various Solutions That Were Used for the Preparation of the Nanofibers via Electrospinning<sup>a</sup>**

Formulation	Chitosan (w/v %)	PVA (w/v %)	PEO (w/v %)	Acetic Acid (w/v %)	VAN (mg/ml)	Flow rate (ml/h)	Viscosity (Pa s)	Distance (cm)	Voltage (kV)
F1	2%	4%	0%	50%	1 mg/ml	0.4 ml/h	4.1	10 cm	15 kV
F2	2%	4%	0%	50%	10 mg/ml	0.4 ml/h	2.6	10 cm	15 kV
F3	2%	0%	2%	50%	1 mg/ml	0.5 ml/h	10.4	12 cm	17 kV
F4	2%	0%	2%	50%	10 mg/ml	0.5 ml/h	12.8	15 cm	30 kV

<sup>a</sup>Viscosity values represented here were obtained from the rheological measurements (flow curves in Figure 4) performed at room temperature, at a shear rate of  $10\text{ s}^{-1}$ .

In this framework, our study aims to develop a drug delivery system utilizing the electrospinning technique. Widely adopted in the biomedical field for its versatility and ability to produce micro- and nanofibers, electrospinning results in a high surface-area-to-volume ratio and a tunable porous structure, facilitating cell attachment, proliferation, and differentiation.<sup>31–34</sup> Thus, it finds numerous applications in tissue engineering, wound healing, and drug delivery. Our project is seated at the intersection of these three categories. The objective of this study was to create a nanofibrous coating for vascular grafts to prevent infections. This was achieved by creating a polymer blend using chitosan, a natural polymer with intrinsic antimicrobial properties, and vancomycin (VAN), a potent antibiotic effective against Gram-positive bacteria. Chitosan's biocompatibility and biodegradability make it an ideal candidate for biomedical applications within the body, minimizing long-term risks.<sup>35,36</sup> Its ability to promote drug release, directly at the target site, enhances therapeutic efficacy while reducing systemic side effects.<sup>37,38</sup> Additionally, to enhance the antimicrobial properties of the nanofibrous coating, vancomycin (VAN) was combined with chitosan. VAN, effective against bacteria often involved in VGI, enhances the coating's efficacy against these pathogens.<sup>39,40</sup> Recent studies have demonstrated vancomycin's enhanced performance when delivered locally, thereby maximizing its therapeutic potential while minimizing systemic toxicity.<sup>41–43</sup> Our approach synergizes the antimicrobial properties of chitosan with the targeted action of vancomycin, proposing a novel and effective strategy for VGI prevention. This combined application is designed to ensure a sustained release of VAN, providing prolonged protection against infection at the graft site, a critical aspect in postsurgical recovery and patient outcomes.

## MATERIALS AND METHODS

**Materials.** Vancomycin HCl was purchased from Tocris Bioscience (Minneapolis). Chitosan medium molecular weight (Mw 47,000 Da), poly(vinyl alcohol) (PVA; Mw 146,000–186,000 Da), poly(ethylene oxide) (PEO; Mw 600,000), and ammonium dihydrogen phosphate were purchased from Sigma-Aldrich (Burlington). Glacial acetic acid high-performance liquid chromatography (HPLC) grade, dimethylformamide (DMF), hexafluoroisopropanol (HFIP), dichloromethane (DCM), and acetone were purchased from Thermo Fisher Scientific (Waltham). Poly(lactic-co-glycolic acid) (PLGA) 50:50 was purchased from Durect (Cupertino).

**Preparation of the Electrospinning Solutions.** The electrospinning solutions were prepared using two different methods depending on the copolymer utilized. We evaluated several iterations, employing either PVA or PEO, and incorporating two distinct concentrations of VAN. Formulations 1 and 2 consisted of a blend of chitosan at 2% w/v, PVA at 4% w/v, and two varying concentrations of VAN: 1 and 10 mg/mL, respectively. Similarly, formulations 3 and 4 contained a blend of chitosan at 2% w/v, PEO at 2% w/v, with VAN concentrations of 1 and 10 mg/mL.

Formulations 1 and 2 were created by dissolving chitosan and PVA separately in a 50% (w/v) acetic acid solution. The chitosan was stirred on a plate overnight at room temperature, while PVA was mixed in a vacuum oven at 90 °C for 6 h under stirring conditions. All vials were sealed with a parafilm to prevent evaporation during stirring. Once fully solubilized, the two solutions were combined, and VAN was added 4 h later. The electrospinning solution was then stored and stirred at room temperature until it was used for electrospinning. Formulations 3 and 4 followed a similar process, with chitosan and PEO being dissolved separately in a 50% (w/v) acetic acid solution, and both compounds were dissolved at room temperature before being combined as previously described.

The PLGA polymeric solution was prepared by dissolving 2 g of PLGA pellets in a mixture of 40% (v/v) DMF and 60% (v/v) acetone, followed by stirring at room temperature overnight.

**Preparation of the Electrospun Coating.** The nanofibrous coating was produced by using the electrospinning technique. In brief, a high-voltage DC power supply (Linari Biomedical, ITA) was set up in an insulating hood along with a flat collector and a syringe pump. The electrospinning solution was loaded into a 20 mL glass syringe (Hamilton) fitted with a 20 G blunt needle. To initiate spinning, both the collector and the syringe needle were connected to the negative and positive poles to create the necessary electric field for nanofiber deposition. Numerous attempts were made to spin chitosan alone at different concentrations (i.e., 3, 6, and 9 mg/mL) dissolved in acetic acid solution (ranging from 10 to 70 v/v %), as well as chitosan (3, 6, and 9 mg/mL) dissolved in HFIP. The flow rates varied from 0.2 to 1.5 mL/min, with applied voltages ranging from 10 to 30 kV, and needle-collector distances from 8 to 20 cm, including all corresponding permutations. Achieving a homogeneous fiber deposition was nearly impossible, leading us to explore the addition of copolymers such as PVA and PEO to enhance the electrospinnability of chitosan, as extensively reported in the literature.<sup>44–47</sup> In fact, chitosan alone proved to be extremely difficult to spin due to its limited solubility.<sup>45,46</sup> Soluble only in acidic solvents such as formic or acetic acid, chitosan becomes a cationic polyelectrolyte in such environments, transforming  $\text{NH}_2$  groups into  $\text{NH}_3^+$ . In an electric field, strong repulsive forces between these positively charged groups prevent the continuous formation of chitosan fibers, resulting in irregular beaded structures. Furthermore, robust hydrogen bonding

between  $\text{NH}_2$  and OH groups in chitosan solutions affects its properties.<sup>44</sup>

At low chitosan concentrations, there are insufficient polymer chains to support fiber formation. However, as the polymer concentration increases, the strengthened hydrogen bonds between the chains create a highly viscous 3D network structure. This dense structure is challenging to electrospin, and to overcome this limitation, researchers have leveraged the use of guest polymers like PVA and PEO to enable the electrospinning of chitosan, achieving great results in terms of fiber formation and homogeneity. By blending, chitosan nanofibers can be obtained with high reproducibility, although the resulting fibers contain not only chitosan but also the guest polymer. Other groups have attempted to reduce repulsion between chitosan chains using harsh reagents, such as DCM and trifluoroacetic acid. While this approach yields pure chitosan nanofibers, the use of harmful solvents limits their clinical application. Therefore, in our study, we opted to fabricate chitosan nanofibers by blending chitosan with PVA and PEO.

The electrospinning solutions used in this work and described in the previous section were loaded in the syringe, and different voltages were applied as described in Table 1. The distance between the needle tip and the collector was adjusted accordingly. The feed rate of the syringe pump (New Era Pump System Inc.) is described in Table 1 as well as the needle-collector distance and voltage applied. The electrospinning process was performed at room temperature and a relative humidity of 60–65%.

**Characterization of Electrospinning Solutions.** Rheological properties of each formulation were assessed using an MCR302 Rheometer (Anton Paar, Austria) equipped with a parallel plate system PP25/P2 (25 mm diameter) and a Peltier chamber to control the temperature with a temperature gradient lower than 0.2 °C during the tests. Rotational and oscillatory tests such as viscosity tests, amplitude sweeps, frequency sweeps, and shear tests were performed to evaluate the viscoelastic properties of the different blends. Viscosity tests performed at different temperatures ranging from 10 to 30 °C were used to evaluate how temperature affects the overall viscosity of the solutions. Amplitude sweeps, with shear strains ranging from 0.01 to 100%, were used to determine the linear viscoelastic region (LVER) by applying an angular frequency of 10 rad/s. Frequency sweep tests were performed to describe the time-dependent behavior of the formulations, providing a preliminary conditioning on the sample by applying a preshear of 100  $\text{s}^{-1}$  for 60 s to erase the previous shear history of the sample. Angular frequencies ranging from 0.1 to 100 rad/s were applied to the samples, with a fixed shear strain applied equal to 0.07% to stay within the LVER previously determined with the amplitude sweep tests.

**Surface Tension Evaluation of the Electrospinning Solutions.** A pendant drop test was performed on each formulation to understand how different solutions and different concentrations of polymers could affect the electrospinnability properties. For this test, an optical tensiometer was used (Biolin Scientific). Static interfacial tension was measured by fitting the Young–Laplace equation by image processing from the value of the difference between the contour shape and density of the droplet created from the needle tip.<sup>48</sup>

**Characterization of Nanofibers. Morphology and Size.** The morphology and the size of the nanofibers were assessed by using a scanning electron microscope (SEM) (NovaNano-

SEM 230, FEI). Samples of the nanofibrous mats were harvested and coated with platinum–iridium (Pt–Ir) using a sputter coater (Cressington). After Pt–Ir coating, the samples were examined with an accelerated voltage of 5 kV–8 kV. The diameter of the nanofibers was inferred by evaluating the SEM images obtained using ImageJ.

**Properties of the Nanofibrous Mats.** Fourier transform infrared spectroscopy (FT-IR, Spectrum BX, PerkinElmer) and thermogravimetric analysis (TGA, CT, PerkinElmer instruments) were performed on samples of the nanofibrous mats. Chemical analysis using FT-IR was performed in the range of 400–4000  $\text{nm}^{-1}$  at room temperature. TGA was performed under a nitrogen atmosphere. The characteristic TGA profiles were recorded between 25 and 500 °C at a constant rate of 10 °C/min.

**Contact Angle Measurements.** The hydrophilicity/hydrophobicity of the nanofibrous mats was assessed using sessile drop measurement, where a droplet of water was placed on the surface of the nanofibrous mat. The static contact angle was then defined by fitting the Young–Laplace equation around the droplet using built-in software provided by Biolin Scientific.<sup>48</sup>

**Drug Loading and Drug Entrapment Efficiency.** The amount of VAN entrapped in the nanofibrous mats was quantified by HPLC. A known mass of the nanofibrous samples (ranging from 6 to 20 mg according to each region) was dissolved in 5 mL of 0.1 M dichloromethane solution. The amount of VAN in the solution was calculated by HPLC at  $\lambda = 205 \text{ nm}$ .

The amount of VAN entrapped in the nanofibrous mats was calculated by comparing the released mass of VAN (wHPLC) from the nanofibrous mat and the mass of VAN dissolved before the electrospinning procedure (wES).

The drug entrapment efficiency of the nanofiber (EE) was calculated by eq 1

$$\text{EE}(\%) = (\text{wHPLC}/\text{wES}) \times 100 \quad (1)$$

Each experiment was performed using at least 3 different replicates, and the average values and standard deviations are reported.

**Release Kinetics of VAN-Loaded Chitosan Nanofibrous Coating (CNC).** The release kinetics of VAN from the CNC *in vitro* was evaluated using HPLC. VAN-loaded CNC mats were sectioned into 16 regions ( $2.5 \times 2.5 \text{ cm}^2$ ) and placed separately in a vial filled with 2 mL of phosphate-buffered saline (PBS). The vials were sealed with parafilm and placed on a shaker in an incubator at 37 °C. At predetermined time intervals, 1 mL of volume was withdrawn for analysis and replaced with new PBS. VAN release was determined using an HPLC method developed by building upon an existing method reported in the literature.<sup>49</sup> A Waters 2695 Alliance Separation module was used. The resulting signals were processed with built-in software (Empower, Waters, Milford). The elution was performed on a Luna C18 5  $\mu\text{m}$  4.6  $\times$  150  $\text{mm}^2$  Phenomenex column. Ammonium dihydrogen solution, 2.6 M, was used as the mobile phase, with a pH of 2.2. The isocratic elution buffer was composed of an 88% mobile phase and 12% acetonitrile. UV detection was performed at 205 nm and 15 min of retention time. The injection volume was 10  $\mu\text{L}$ . Calibration curves for VAN were constructed over the range of 1.95–2 mg/mL of VAN in Milli-Q water. The limit of quantification was 0.5  $\mu\text{g}/\text{mL}$ .

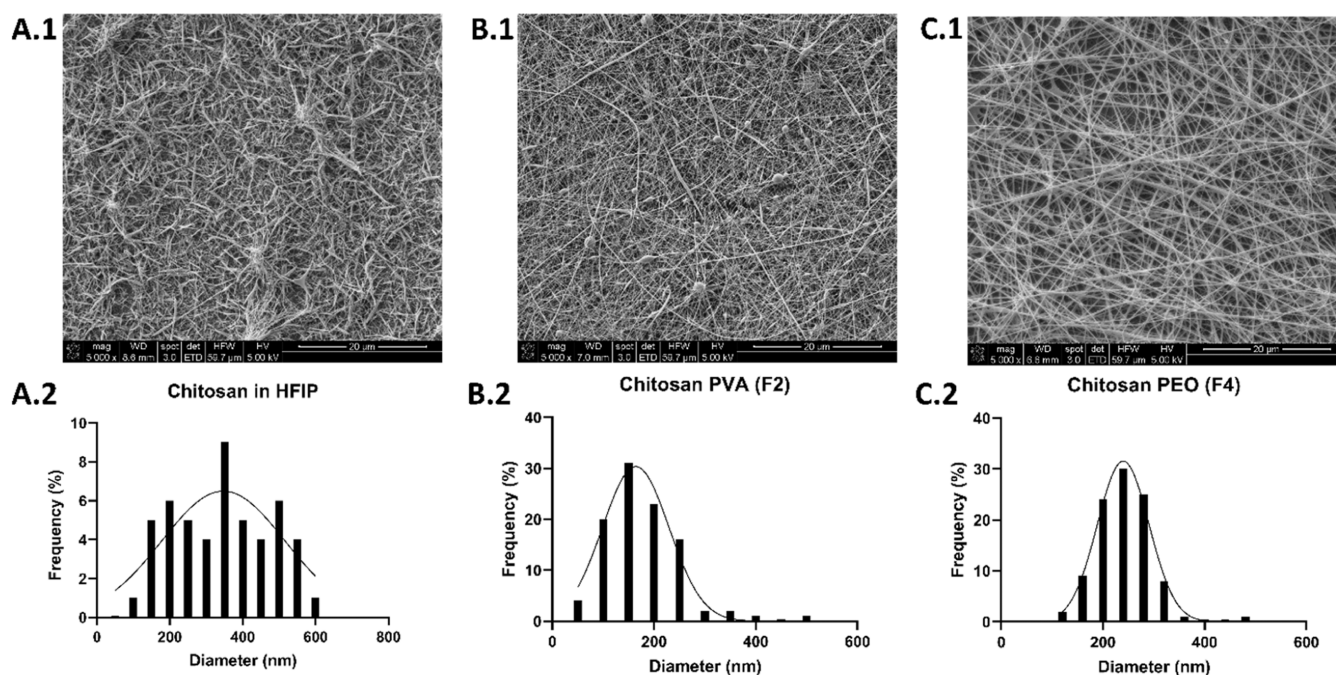


**Figure 1.** Microscopic characterization of nanofibrous mat SEM images of formulations of vancomycin nanofibers at magnifications of 5000x and corresponding size distribution histograms. (A) Formulation with chitosan in HFIP. (B) Formulation with chitosan and PVA in acetic acid solution (F2). (C) Formulation with chitosan and PEO in acetic acid solution (F4). Chitosan alone proved to be extremely difficult to spin due to its limited solubility (A), and for this reason, the addition of a copolymer such as PVA and PEO was explored to enhance the electrospinnability properties of chitosan (B,C).

**Biocompatibility Assessment.** Human umbilical vein endothelial cells (HUVECs) were cultured in endothelial cell growth basal medium-plus (Lonza, no. CC-5036) according to the manufacturer's specification. Patches were cut to a diameter of 6 mm using a biopsy punch and coated with gelatin-based coating solution (Cell Biologics, #6950) via incubation at room temperature for 10 min. HUVEC cells ( $5 \times 10^3$ ) were seeded onto patches in 20  $\mu\text{L}$  droplets and incubated for 1 h to aid attachment before patches were covered with media and incubated for 24 h at 37  $^\circ\text{C}$ . Following incubation, viability was assessed via immunofluorescent staining with 2  $\mu\text{M}$  calceinAM and 8  $\mu\text{M}$  ethidium homodimer. Z-stack images were acquired at 10 $\times$  magnification using the A1 Nikon Confocal Imaging System (Nikon Corporation, Tokyo, Japan). Z-stacks were composed of  $\geq 25$  images at 15  $\mu\text{m}$  intervals.

**Statistical Analysis.** Statistical analysis was performed on all of the results shown in the manuscript, from the SEM evaluation to TGA, FT-IR analysis, and release kinetics of each section. Results are reported as mean values  $\pm$  standard deviation obtained from 3 different replicates. Differences were considered statistically significant for  $P$  values  $< 0.05$ . GraphPad Prism 8.4.3 was used to analyze and plot all data.

## RESULTS AND DISCUSSION

**Microscopic Characterization of Different CNC Candidates.** Chitosan is a natural polymer with intrinsic antibacterial properties,<sup>50–52</sup> which should make it amenable for tissue engineering applications, but its high molecular weight, high viscosity, and low solubility have hindered its use.<sup>53,54</sup> Additionally, chitosan tends to form aggregates or clumps, and this is one of the most concerning issues in electrospinning because it prevents the formation of continuous fibers. For this reason, several preliminary

evaluations were conducted using different solvents and copolymers. In Table 1, an overview of the different iterations is reported. As mentioned earlier in the Materials and Methods section, the use of guest polymers, easy to spin such as PVA and PEO, has shown great results in terms of fiber formation and homogeneity.<sup>55,56</sup> By blending, chitosan becomes easier to electrospin, and nanofibrous mats with homogeneous characteristics can be obtained. For this reason, different concentrations of PVA and PEO were investigated following the various examples reported in the literature,<sup>44,45,57</sup> and in Table 1, the final concentrations chosen for our study are reported.

Formulations F1 and F2 are characterized by the same concentrations of chitosan and PVA but two different concentrations of VAN dissolved within the polymeric solutions, respectively 1 and 10 mg/mL. Formulation F3 and F4 instead are composed of the same concentrations of chitosan and PEO but two different concentrations of VAN, respectively, 1 and 10 mg/mL. For each formulation, a summary of the electrospinning parameters used is reported.

Our initial experiments involved using chitosan solutions of 3, 6, or 9% (w/v) in HFIP, followed by trials with chitosan in DCM. Subsequently, we explored blending chitosan with copolymers (PVA or PEO) in acidified water. We tested various copolymer concentrations employing different levels of acidified water as the solvent. It was observed that increasing the copolymer concentration facilitated chitosan's solubility. To further enhance solubility, we varied the acetic acid concentration from 10% to 90% w/v. However, higher acetic acid levels led to increasing the opaqueness in the solution. Consequently, we selected a 50% w/v concentration of acetic acid, which was found to improve solubility and maintain the solution's clarity while enhancing the volatility of the final polymer solution.

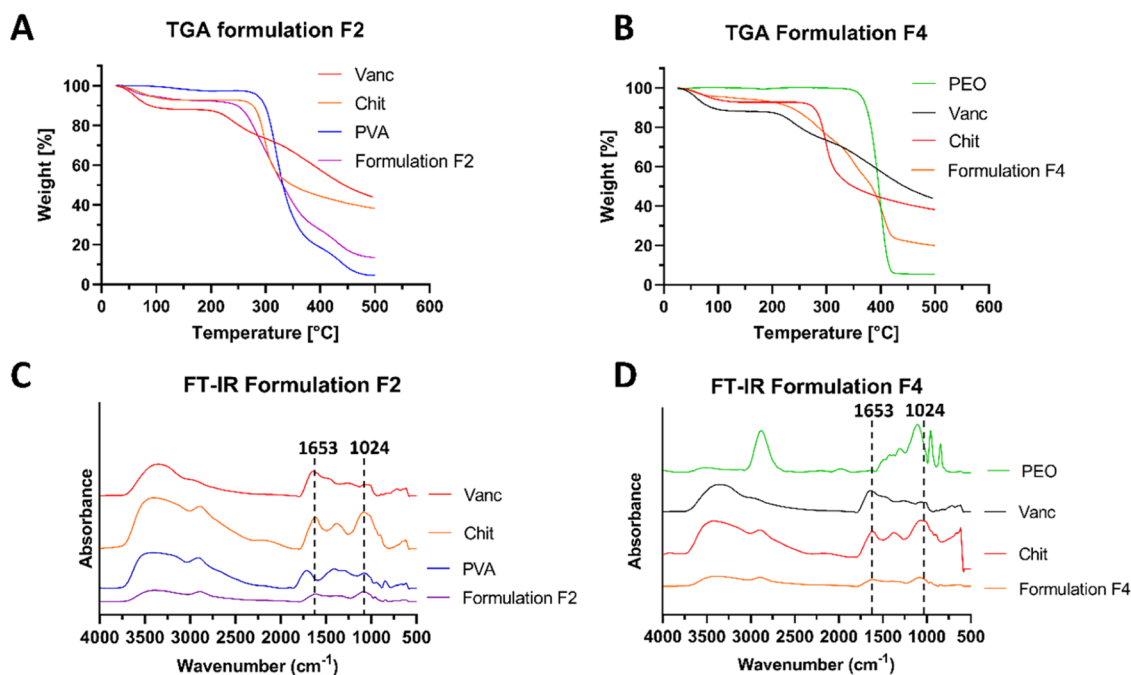


**Figure 2.** TGA and FT-IR characterization from the TGA curves of formulations F2 and F4 (A, B), three characteristic temperature intervals of weight loss can be inferred. The first region (50–100 °C), with 10–15% weight loss, corresponds to the evaporation of water content. The second weight loss, occurring in the range of 200–250 °C, is the result of VAN degradation and accounts for 10–15% of weight loss. This is in accordance with the overall mass of VAN dissolved in the polymeric solution. The last stage, at temperatures higher than 250 °C, is characterized by the degradation of chitosan at 250 °C, PVA at 280 °C, and PEO at 350 °C. The characteristic inflection points observed in the TGA curves demonstrated the presence of VAN within the nanofibrous membrane. FT-IR analysis (C, D) also showed the presence of VAN, with the amide peak at 1653  $\text{cm}^{-1}$  and the characteristic peak at 1024  $\text{cm}^{-1}$  of the amine stretching. These peaks were partially covered by the same peaks present in the chitosan.

The nanofibrous mat obtained with chitosan in HFIP without copolymers showed a heterogeneous deposition with defects due to the formation of clumps and aggregates (Figure 1A). The frequency distribution of the diameters was characterized by a high standard deviation ( $347 \pm 169$  nm). Instead, once copolymers were added (formulations F1, F2, F3, and F4), a homogeneous deposition was obtained (Figure 1B,C). Formulation with PVA was characterized by an average diameter size of ( $164.1 \pm 65.34$  nm). Fiber diameters showed a Gaussian size distribution, as reported in the charts at the bottom line of Figure 1. Interestingly, the blend composed with PEO showed a homogeneous deposition as well, with an average diameter size of ( $240 \pm 50.81$  nm) with fewer beads and defects compared to the nanofibers with PVA.

According to the results of these SEM images, we decided to perform a deeper characterization of formulations with PVA and PEO. Four different formulations were prepared, consisting of chitosan and PVA with 1 and 10 mg/mL VAN (formulations F1 and F2, respectively) and chitosan and PEO with 1 and 10 mg/mL VAN (formulations F3 and F4, respectively). Chitosan has limited solubility in common organic solvents, which makes it challenging to obtain a homogeneous spinning solution.<sup>58</sup> Since chitosan is a polycationic polymer, and its solubility is influenced by pH, it is more soluble in acidic conditions due to the protonation of amino groups, which is why we used acetic acid.<sup>59,60</sup> Incorporating drugs into chitosan nanofibers while maintaining their stability and bioactivity can be challenging.<sup>61–63</sup> Some drugs may have limited solubility in the spinning solution, affect the electrospinning process, or degrade during the process. Ensuring proper drug encapsulation and controlled

release is essential.<sup>64</sup> Moreover, tuning the quantity of vancomycin embedded within the coating is important for translational approaches. The selected concentrations of VAN loaded within the nanofibrous coatings (1 and 10 mg/mL) were chosen after taking into consideration what was already available in the clinical settings. VAN administration depends on several aspects such as specific product composition, clinical application, and route of administration.<sup>65,66</sup> These considerations must be paired with the patient's health history and the presence of comorbidities, such as diabetes and cardiovascular pathologies, which can increase the risks of bacterial infections.<sup>17,67</sup>

The gold standard relies on the systemic intravenous administration of VAN with concentrations ranging from 0.5 to 5 mg/mL or 15–20 mg/kg if weight-based, depending on the gravity of the infection and patient's body weight.<sup>68–70</sup> In surgical settings, vascular grafts are commonly presoaked in vancomycin solutions with concentrations ranging from 5 to 10 mg/mL as a preventive measure.<sup>71</sup> A broad range of concentrations demonstrates a lack of clarity and a clear indication. Moreover, our study aims to achieve a localized release of VAN, at the site that is more susceptible to infection. With intravenous and oral administration of VAN, the amount of drug needed is higher due to the systemic approach used. As far as we know, no clear evidence exists and sufficient clinical data to support the effective local dosage using similar devices like the one we developed. However, we are currently assessing, through a clinical trial, toxicity limits and efficacy of local delivery of VAN in patients undergoing total hip and total knee arthroplasty following an approach similar to the one presented here.<sup>72</sup>

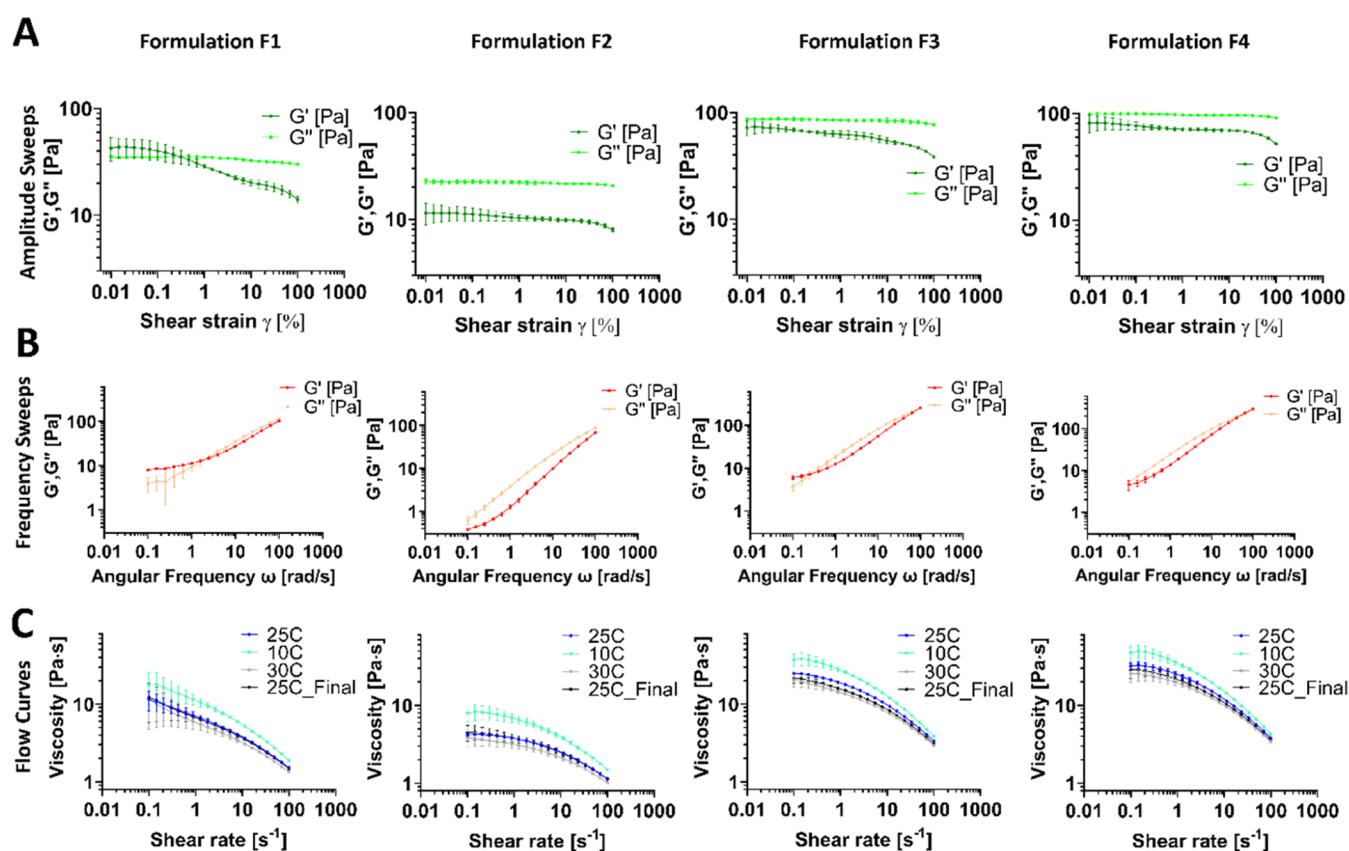


**Figure 3.** Rheological characterization of formulations F1, F2, F3, and F4. Amplitude sweep tests were performed preliminarily (A) to identify the LVER. For formulation F1, a value of a 0.1% shear strain was identified as the upper limit for the LVER, while for formulations F2, F3, and F4, a shear strain of 1% was chosen to stay within the LVER. Frequency sweep tests were performed to evaluate the behavior of the different formulations in the oscillatory regimen to determine the time-dependent characteristics of each formulation (B). F2 and F4 formulations show substantial parallelism of the  $G'$  and  $G''$  curves, with loss modulus  $G''$  being above the storage modulus  $G'$ . Conversely, formulations F1 and F3 reveal a crossover, occurring at approximately 1 rad/s for F1 and 0.4 rad/s for F3. Flow curves at different temperatures were performed sequentially to evaluate how viscosity was affected by different shear rates and temperatures (C). An increase in the shear rate resulted in a decreased viscosity. This shear thinning behavior was observed in all four formulations for shear rates above 1–10 s<sup>-1</sup>. For shear rates below 1 s<sup>-1</sup>, all samples approached a Newtonian plateau.

**TGA and FT-IR Characterization.** After obtaining the nanofibrous mat, we performed elemental analysis of the electrospun material, as shown in Figure 2. The TGA curves of formulations F2 and F4 (Figure 2A,B) reveal three characteristic temperature intervals of weight loss. In the first region (50–100 °C), which shows a 10–15% weight loss, the loss corresponds to the evaporation of water content. The second stage of weight loss, occurring between 200 and 250 °C, is attributed to VAN degradation and accounts for another 10–15%. This is in accordance with the overall mass of VAN dissolved in the polymeric solution. The final stage, occurring at temperatures above 250 °C, involves the degradation of chitosan at 250 °C, followed by PVA at 280 °C and PEO at 350 °C. The characteristic inflection points observed in the TGA curves demonstrated the presence of VAN within the nanofibrous membrane. The FT-IR analysis (Figure 2C,D) confirmed the presence of VAN, indicated by the amide peak at 1653 cm<sup>-1</sup> and the characteristic amine stretching peak at 1024 cm<sup>-1</sup>. However, these peaks partially overlap with similar peaks found in chitosan.

**Rheological Assessment.** Rheological characterization was performed to gather more data on the viscoelastic properties of polymeric solutions F1, F2, F3, and F4. Preliminary amplitude sweep tests (Figure 3A) were

conducted to identify the LVER. For formulation F1, a value of 0.1% shear strain was identified as the upper limit for the LVER, while for formulations F2, F3, and F4, a shear strain of 1% was chosen to stay within the LVER. Frequency sweep tests were performed to evaluate the behavior of the different formulations in the oscillatory regimen (Figure 3B). F2 and F4 formulations show substantial parallelism of the  $G'$  and  $G''$  curves, with loss modulus  $G''$  being above the storage modulus  $G'$ . Conversely, formulations F1 and F3 revealed a crossover, occurring at approximately 1 rad/s for F1 and 0.4 rad/s for F3. This crossover is accompanied by an increase in modulus  $G'$  surpassing the values of loss modulus  $G''$  at lower frequencies. These findings suggest that at low frequencies, formulations F1 and F3 exhibit a more elastic response, but this behavior changes as the frequency increases. Formulations F2 and F4 always showed a moderate preponderance of the viscous response in the entire range of frequencies investigated. A possible crossover might also be present for F2 and F4 at very low frequencies (below 0.1 rad/s), i.e., below the range of our interest here investigated. All samples (F1–4) at the upper edge of frequencies investigated show the two curves approaching each other. Also, in this case, the eventual presence of a high-frequency crossover (above 100 rad/s) is of

limited interest to our application and was not further investigated.

Flow curves at different temperatures were performed sequentially to evaluate how the viscosity was affected by different shear rates and temperatures. As described in Figure 3C, an increase in shear rate resulted in decreased viscosity. This shear thinning behavior was observed in all four formulations for shear rates above  $1\text{--}10\text{ s}^{-1}$ . For shear rates below  $1\text{ s}^{-1}$ , all samples approached a Newtonian plateau. Interestingly, at  $10\text{ }^{\circ}\text{C}$ , the overall viscosity was higher than at  $25\text{ or }30\text{ }^{\circ}\text{C}$  (Figure 3C); this could be due to the partial rearrangement of the water molecules present in each formulation.

Additionally, complex viscosity ( $\eta^*$ ) obtained from the frequency sweep measurements and steady-state shear viscosity ( $\eta$ ) obtained from flow curves were evaluated to check whether the Cox–Merz rule could apply to the four formulations, simplifying the comparison between these two different rheological measurements. The Cox–Merz empirical rule could theoretically apply only to formulation F2, while for all of the other formulations, no marked correlation was observed except for angular frequencies/shear greater than  $10\text{ rad/s}^{-1}$  (Figure S1).

The viscoelastic properties of a polymeric solution play a crucial role in assessing its suitability for electrospinning, a widely used technique to produce nanofibrous materials.<sup>73,74</sup> There is a correlation between polymer viscosity and electrospinnability, as the viscosity of the polymer solution significantly impacts the electrospinning process and the resulting fiber morphology.<sup>75</sup> A solution with an appropriate viscosity enables the continuous and controlled extrusion of the polymer through the spinneret or needle. If the viscosity is too low (i.e.,  $\eta < 100\text{ mPa}\cdot\text{s}$ ), the solution may form droplets or beads instead of fibers.<sup>74,76</sup> On the other hand, if the viscosity is too high (i.e.,  $\eta \gg 10\text{ Pa}\cdot\text{s}$ ), the solution may have difficulty flowing and the electric field generated by a laboratorial electrospinning setup is not sufficient to form uniform fibers.<sup>77</sup> Therefore, an optimal viscosity range is necessary for successful fiber formation.<sup>78</sup> Moreover, the polymer viscosity affects the uniform distribution of the polymer within the solution.

While viscosity is commonly regarded as the primary rheological parameter to be evaluated, in our specific process, the viscoelasticity of the fluids plays a pivotal role, as highlighted, for instance, in Castellano et al.<sup>74,79</sup> For this reason, a comprehensive rheological characterization, particularly in the LVER, is needed and is best accomplished through amplitude sweep and frequency sweep tests.<sup>80,81</sup> In particular, the LVER can be determined only after performing amplitude sweep measurements, applying different shear strains on the polymeric solutions, and evaluating their response.<sup>82,83</sup> On the other hand, frequency sweep tests are necessary for describing the viscoelastic properties of the different formulations in the oscillatory domain. These tests involve the application of a fixed strain within the previously determined LVER, obtained from the amplitude sweep tests. Frequency sweep tests were performed to replicate the dynamic deformation experienced by the solution as it is extruded through the syringe needle during the electrospinning process.<sup>81</sup>

Ensuring the uniformity of solutions is crucial for achieving consistent properties in electrospun fibers. Conducting rheological assessments before the electrospinning process,

particularly for composite solutions with diverse properties, holds great importance, and understanding the behavior of polymer solutions across a range of frequencies is fundamental.<sup>79,84</sup> Identifying how the solutions respond to dynamic deformation, such as those encountered during the electrospinning process, can provide valuable insights. In our study, the absence of crossover in the storage modulus ( $G'$ ) and loss modulus ( $G''$ ) curves in the tested frequency range ( $0.1\text{--}10\text{ rad/s}$ ) suggests a liquid-like behavior for the polymer solution.<sup>85–87</sup> The solution's ability to maintain a consistent, liquid-like behavior at different frequencies is desirable for producing uniform fibers during the electrospinning process.<sup>81</sup> The subsequent microscopic evaluation of the nanofibrous coatings obtained from formulations F2 and F4 showed higher reproducibility of nanofibers with an average diameter of ( $164.1 \pm 65.34\text{ nm}$ ) and ( $240 \pm 50.81\text{ nm}$ ), respectively, endorsing the findings observed during the rheological characterization. Moreover, a higher concentration of VAN dissolved within the two polymeric solutions made F2 and F4 more amenable for further characterization since the healing process of surgical wounds usually takes at least 14 days. Being able to effectively embed higher concentrations of VAN would be beneficial to achieving a controlled and sustained release of VAN for a longer period of time.

**Surface Tension of the Polymeric Solutions.** The electrospinning technique is based on the application of an electric field to a polymeric solution pumped through a needle to create instability, impose monoaxial stretching of the extruded fluid, and generate a nanofibrous thread to be spun onto a specific target (collector). Therefore, in characterizing a polymeric solution for electrospinning, both rheological parameters and surface tension play crucial roles.<sup>88,89</sup> Surface tension was assessed to gauge the difficulty an electric field faces in overcoming the cohesive forces at the molecular level within a specific solution. The higher the surface tension, the higher the electric field needs to be to create instability and generate nanofibers.<sup>90,91</sup> Figure 4 presents the evaluation of formulations F1, F2, F3, and F4. The results indicated surface

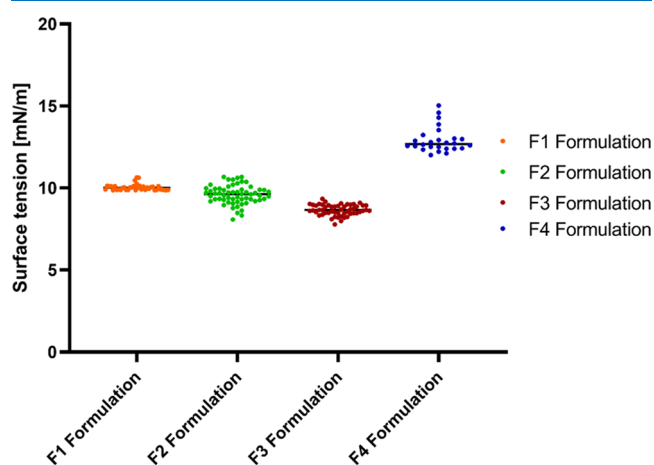


**Figure 4.** Evaluation of surface tension for polymeric blends. The surface tension of the solution affects the jet's ability to stretch and form fibers, as well as the resulting fiber morphology. A lower surface tension generally leads to thinner and more uniform fibers. On the other hand, higher surface tension can result in thicker and less uniform fibers due to reduced stretching of the jet. Surface tension values of around  $8.5\text{--}10\text{ mN/m}$  for the first three formulations were observed, while formulation F4 had a surface tension of  $13.2\text{ mN/m}$ .

tensions of approximately 8.5 and 10 mN/m for the first three formulations, whereas formulation F4 exhibited a surface tension of 13.2 mN/m.

These results are in accordance with the differences in voltage applied to the polymeric solution during the electrospinning process, as reported in Table 1. While formulations F1, F2, and F3 had comparable values of voltage applied to obtain nanofibrous deposition, formulation F4 required a higher voltage to form nanofibers. The incorporation of PEO and PVA as additives was intended to reduce the surface tension of the polymer solution.<sup>92,93</sup> Indeed, all formulations containing these additives showed enhanced spinnability.

**Hydrophilicity of the Nanofibrous Mats.** Evaluating surface properties, such as hydrophilicity and hydrophobicity, is crucial in the design of new implantable devices as these factors significantly influence their success or failure. Figure 5

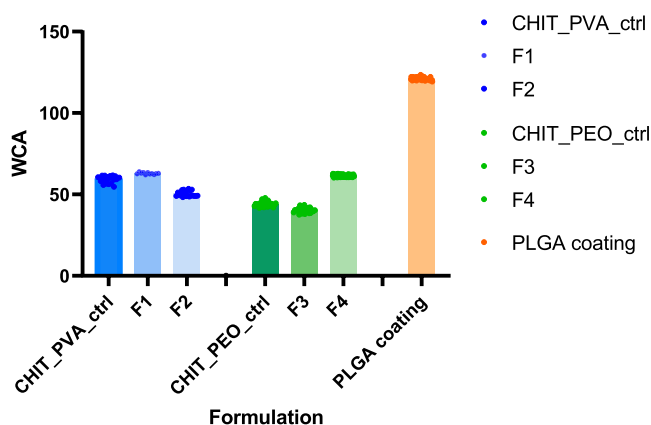


**Figure 5.** Evaluation of surface behavior of the CNC of vascular graft through WCA measurements. Chitosan 2% w/v + PVA 4% w/v in 50% w/v acetic acid solution was used as a control against formulations F1 and F2. Chitosan 2% w/v + PEO 2% w/v in 50% W/V acetic acid solution was used as a control against formulations F3 and F4. PLGA coating spun on top of the vascular graft containing VAN. An overall hydrophilic behavior for the nanofibrous mats was obtained from formulations F1, F2, F3, and F4, suggesting good water affinity with WCA values well below 90°. The PLGA coating deposited on the nanofibrous mats, to enhance the sustained release of VAN, changed the overall affinity of the nanofibrous mats, suggesting a hydrophobic behavior with a WCA equal to 121 ± 2° (mean ± SD).

illustrates that the nanofibrous mats from formulations F1, F2, F3, and F4 exhibit overall hydrophilic behavior, as evidenced by WCA values significantly below 90°, indicating strong water affinity. Water contact angle measurements were performed on the nanofibrous mats after the deposition of the additional nanofibrous PLGA coating to enhance the sustained release of VAN (Figure 5). The PLGA coating changed the overall affinity of the nanofibrous mats, suggesting a hydrophobic behavior with a WCA equal to 121 ± 2° (mean ± SD).

The impact of hydrophilicity and hydrophobicity on biofilm formation is a topic that has undergone extensive exploration; however, its precise influence remains a subject of ongoing discussion. It is well-established that rough surfaces enhance bacterial adhesion, thereby increasing the likelihood of biofilm formation compared to smoother surfaces. Furthermore, the realm of biofilm formation encompasses various contributing factors, including the bonding of chemical entities onto the substrate and the presence of proteins or other biomolecules

within the outer layer.<sup>94,95</sup> Given the complex interplay of these factors, it becomes challenging to isolate and understand the specific roles of hydrophilicity and hydrophobicity. The prevailing belief is that hydrophilic substrates, owing to their high surface energy, may diminish or at least not promote biofilm formation.<sup>96–98</sup> As bacterial cell surfaces generally exhibit hydrophobic properties, biofilm formation is more likely on surfaces that are less wettable and more hydrophobic.<sup>99–101</sup> Nevertheless, conclusive determinations on this subject remain elusive.

#### Kinetics of Release of the Nanofibrous Mats.

Following a detailed assessment of the chemical and surface characteristics of the nanofibrous mats, we examined the kinetics of VAN release. To quantify the VAN release, an HPLC method was developed. The nanofibrous mat was first sectioned into 16 different regions and then soaked in PBS. From the HPLC analysis of each region at specific time points, we obtained heat maps of the overall release of antibiotics from the drug-eluting mat as depicted in Figure 6. In particular, formulations F2 and F4, prepared with a higher VAN content (10 mg/mL), were evaluated. After 30 min, the region that released the most VAN from the PVA-based formulation F2 mat had released 1.75 mg of VAN, and in the PEO-based formulation F4 mat, the highest amount released was 2.75 mg. From 30 min to 1 h, a decrease in release compared to the initial 30 min was observed in both cases, with the highest release measured equal to 0.84 mg for F2 and 0.74 mg for F4. From 1 to 3 h, the highest values released were 1.24 mg (F2) and 1.27 mg (F4). From 3 to 8 h, VAN release reached 0.37 mg (F2) and 0.32 mg (F4). VAN was still released from 8 to 24 h, with highest values of 0.44 mg (F2) and 0.37 mg (F4). The heatmap representation offers a qualitative view of the areas with the highest VAN concentration, providing an estimate of the electrospinning deposition quality. Overall, the nanofibrous deposition was focused more on the central regions, suggesting good targeting of the collector. The same findings were observed for formulations F1 and F3, as represented in Figure S3.

Figure 7 describes more in-depth, from a quantitative standpoint, the values obtained from the HPLC analysis of released VAN from formulations F2 and F4. From the data obtained from the HPLC analysis of the different regions of the nanofibrous mats, the entrapment efficiency was evaluated as described in the Materials and Methods section. The released mass of VAN from the nanofibrous mat was compared to the mass of VAN dissolved in the different formulations before electrospinning. The entrapment efficiency was found to be approximately 50% for formulations F2 and F4. This could be explained by the difficulty in focusing the electrospinning process in a well-confined area. Figure 7A–D represents the cumulative release profile of the nanofibrous mats obtained from formulations F2 and F4 after considering the 50% entrapment efficiency. In particular, a 90% release of VAN was observed for both formulations F2 and F4 after 3 h. The plateau level was reached after 8 h, suggesting a fast release profile (Figure 7A–D). Moreover, two regions in F4:1. A and 1. B, respectively, showed an even faster release profile, with a 95% release after 3 h. This could be explained by the heterogeneous nanofibrous deposition obtained in the 16 sections. Complementary graphs of the cumulative release (Figure 7B–E) and the release profile at each time point (Figure 7C–F) of each section help describe how each section contributed to the overall release and reinforce the findings

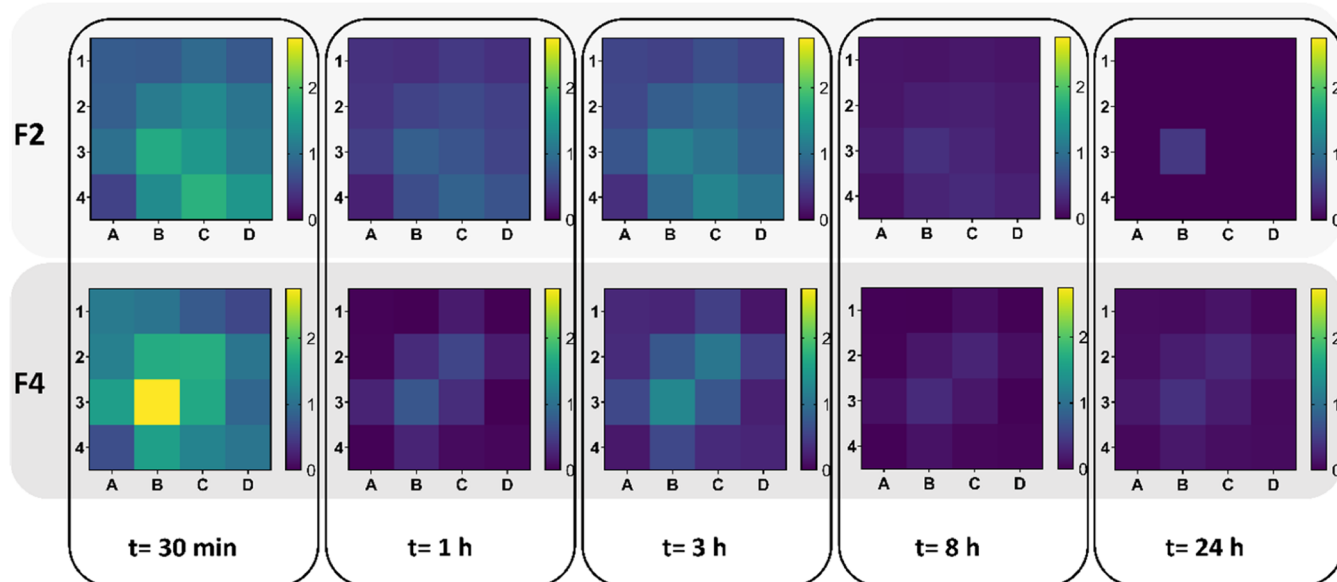


**Figure 6.** Heatmap of the released VAN from the nanofibrous mats obtained with formulations F2 and F4. The heatmap representation gives a qualitative view of the most loaded areas, which provides an estimate of the quality of the electrospinning deposition. Overall, the nanofibrous deposition was focused more on the central regions, suggesting a good targeting of the collector. After 30 min, the region that released the most VAN from the PVA-based formulation F2 mat had released 1.75 mg of VAN, and in the PEO-based formulation F4 mat, the highest amount released was 2.75 mg. From 30 min to 1 h, a decrease in release compared to the initial 30 min was observed in both cases, with the highest release measured equal to 0.84 mg for F2 and 0.74 mg for F4. From 1 to 3 h, the highest values released were 1.24 mg (F2) and 1.27 mg (F4). From 3 to 8 h, VAN release reached 0.37 mg (F2) and 0.32 mg (F4). VAN was still released from 8 to 24 h, with highest values of 0.44 mg (F2) and 0.37 mg (F4).

represented with the heatmap graphs shown in Figure 6. The quantitative analyses confirm that the highest amount of VAN was released from the central regions, with a more sustained release throughout the 24 h, while the contribution of peripheral areas is more marginal. This can be explained by the deposition of nanofibers, mostly in the central regions of the collector. Also, for formulations F1 and F3, the quantitative evaluations represented in Figure S3 showed a higher amount of VAN released from the central regions, corroborating the findings observed from the heat maps in Figure S2, findings that are in accordance with those obtained from formulations F2 and F4. Electrospinning with a horizontal geometry, like the one used for this study, can present certain limitations compared to traditional vertical electrospinning setups. Horizontal electrospinning setups may encounter difficulties in maintaining stable jet formation during the electrospinning process. Gravity can play a role in the stability of the jet and the control of fiber diameter.<sup>102,103</sup> Without the aid of gravity, the jet stability can be compromised, resulting in variations in fiber diameter and bead formation.<sup>104,105</sup> We did achieve good control over the jet stability and the coating uniformity in topography; however, in the horizontal electrospinning, the distribution of the electric field can be less uniform compared to vertical setups. This nonuniformity can affect the electrospinning process, leading to variations in fiber deposition as in this specific case. Despite these limitations, horizontal electrospinning setups can still be used successfully in this type of application if the resulting coating is well-characterized and standardized.

**Kinetics of the Release of the PLGA-Coated Nanofibrous Mats.** Building upon the results obtained from the HPLC analysis and aiming for a more sustained release of antibiotics for a longer period of time, we added an additional layer of PLGA, using it as a coating. The PLGA deposition was

carried out as described in a previous work from our group.<sup>106,107</sup> The nanofibrous coating in PLGA was electrospun on top of the nanofibrous mats already made obtaining a homogeneous deposition with fibers of  $177.3 \pm 19.8$  nm (mean  $\pm$  SD) in diameter (Figure S4). HPLC evaluation was carried out using the same method as for noncoated mats. In Figure 8, a heatmap shows the release of VAN from nanofibrous mats obtained from formulations F2 and F4 with the addition of the PLGA coating. The highest values of VAN release for any of the regions at 30 min were 1.36 and 2.03 mg, respectively, for formulations F2 and F4. From 30 min to 1 h, the highest VAN released was 0.23 mg (F2) and 0.47 mg (F4). From 8 to 24 h, maximum release amounts of 0.52 mg (F2) and 0.47 mg (F4) were observed. From 1 to 7 days, VAN was still being released by the more heavily loaded regions of the mats, with the highest values of 0.12 (F2) and 0.1 mg (F4). These results show that after a burst release, there was a sustained release of up to 7 days.

To help distinguish with better accuracy the actual release throughout time, we plotted the cumulative release and release profile of the PLGA-coated mats (Figure 9). The release reached a plateau after 3 days and reached almost 100% of VAN released after 7 days (Figure 9A–D). This suggests that the PLGA layer slows the overall release of antibiotics compared to the complete release obtained in less than 24 h observed in uncoated mats (Figure 7A–D). From the complementary graphs of the cumulative release profile in mass (Figure 9B–E) and the release profile at each time point (Figure 9C–F), we can observe that the release followed an exponential behavior.

Upon assessing the drug delivery mechanism, it was identified that diffusion primarily contributes to the release of VAN. The system exhibits a biphasic nature, characterized by an initial burst release profile, which is the predominant

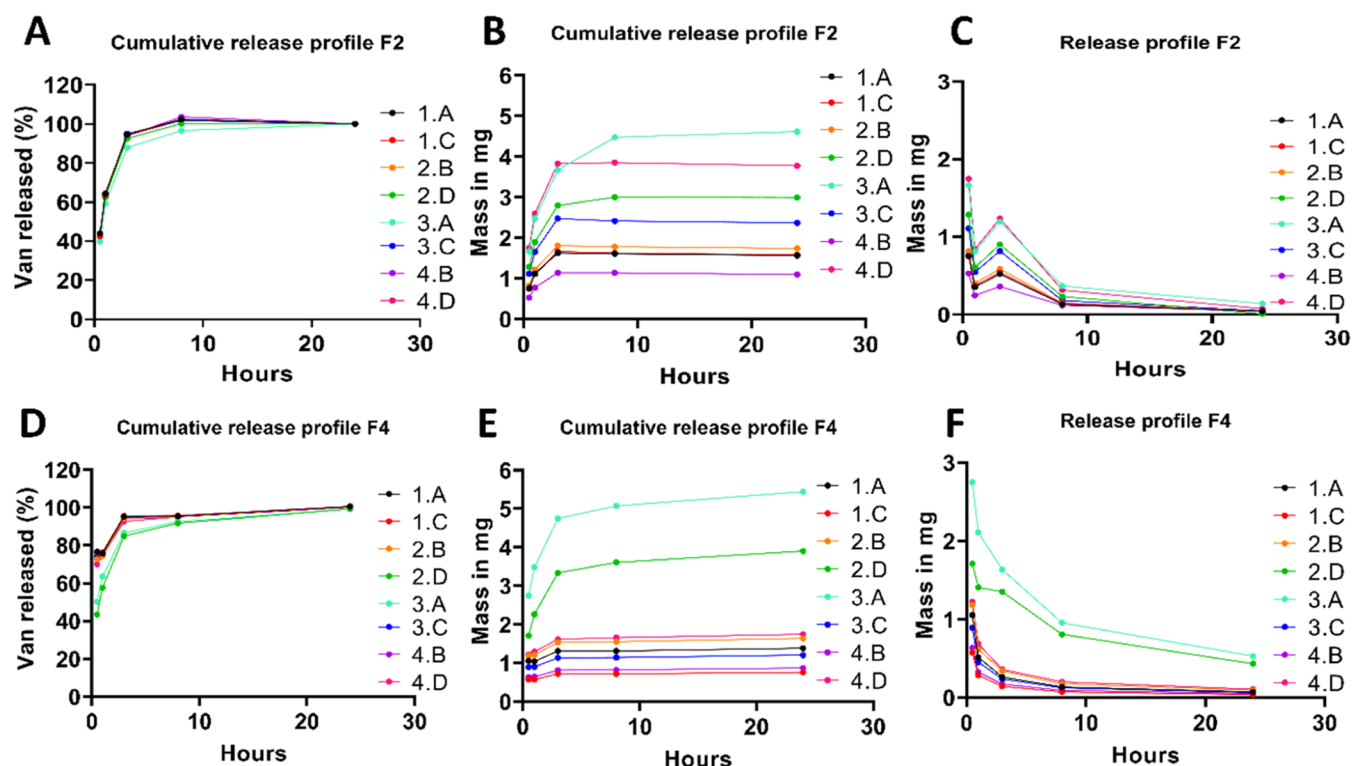


**Figure 7.** Direct quantification with HPLC of the release kinetics from the drug-eluting nanofibrous mats obtained with formulations F2 and F4. Panels (A–D) represent the cumulative release profile of the nanofibrous mats obtained from formulations F2 and F4 after considering a 50% entrapment efficiency. A 90% release of VAN was observed for both formulations F2 and F4 after 3 h. The plateau level was reached after 8 h, suggesting a fast release profile. Moreover, two regions in F4:1. A and 1. B, respectively, showed an even faster release profile, with a 95% release after 3 h. This could be explained by the heterogeneous nanofibrous deposition obtained in the 16 sections. Complementary graphs of the cumulative release (B–E) and the release profile at each time point (C–F) are also enclosed here. The highest amount of VAN was released from the central regions, with a more sustained release throughout the 24 h, while the contribution of peripheral areas is more marginal. This can be explained by the deposition of nanofibers mostly in the central regions of the collector.

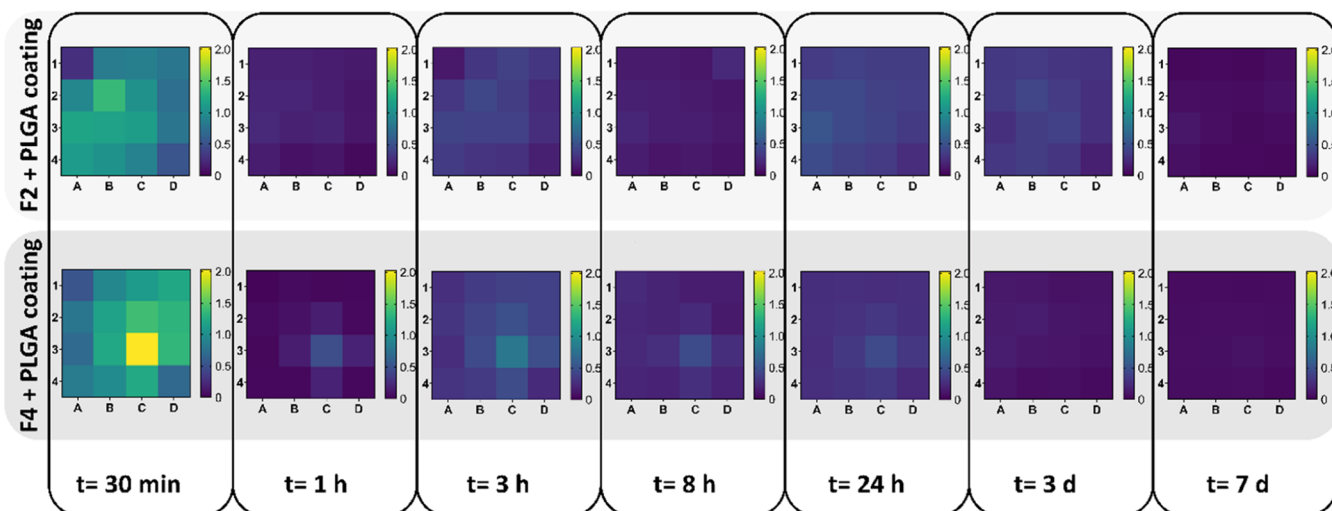


**Figure 8.** Heatmap of the released VAN from the nanofibrous mats obtained with formulations F2 and F4 after adding a coating of PLGA. The highest values of VAN release for any of the regions at 30 min were 1.36 and 2.03 mg, respectively, for formulations F2 and F4. From 30 min to 1 h, the highest VAN released was 0.23 mg (F2) and 0.47 mg (F4). From 8 to 24 h, the maximum release amounts of 0.52 mg (F2) and 0.47 mg (F4) were observed. From 1 to 7 days, VAN was still being released by the more heavily loaded regions of the mats, with the highest values of 0.12 (F2) mg and 0.1 mg (F4). These results show that after a burst release, there was a sustained release of up to 7 days.

mechanism, followed by a rapid release due to erosion of the polymeric coating in PLGA.

The release kinetics studies allowed us to model the release curve using the Korsmeyer–Peppas model that captures the

drug release mechanism for chitosan-based nanocoatings, both with and without the additional PLGA coating.<sup>108</sup> More in detail, the Korsmeyer–Peppas model for drug release is particularly indicated to describe the release kinetics of a drug

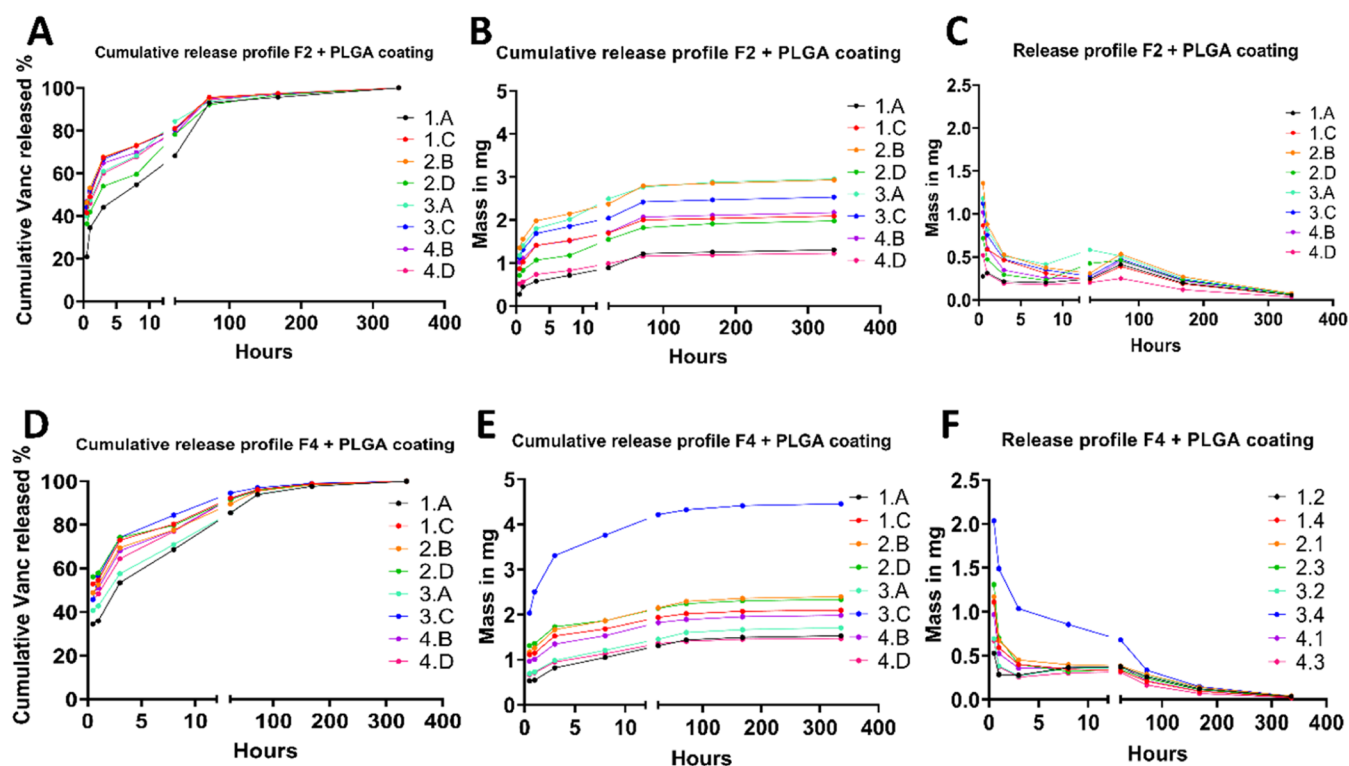


**Figure 9.** Direct quantification with HPLC of the release kinetics from the drug-eluting nanofibrous mats obtained with formulations F2 and F4 after adding a coating of PLGA. The release reached a plateau after 3 days and reached almost 100% of VAN released after 7 days (A–D). This suggests that the PLGA layer slows the overall release of antibiotics compared to the complete release obtained in less than 24 h observed in uncoated mats (Figure 7A–D). From the complementary graphs of the cumulative release profile in mass (B–E) and the release profile at each time point (C–F), we can observe that the release followed an exponential behavior.

**Table 2. Mathematical Parameters Derived from the Korsmeyer–Peppas Equation Describing the Typical Mechanism of Drug Release from a Polymeric System<sup>a</sup>**

formulation	$K$	$M_t$	$M_\infty$
F2	$0.725 < k < 0.899$	$9.35 < M_t < 15.25$	$98.23 < M_\infty < 101.7$
F4	$0.52 < k < 0.628$	$25.19 < M_t < 66.77$	$95.99 < M_\infty < 98.98$
F2 + PLGA	$0.043 < k < 0.088$	$14.73 < M_t < 25.76$	$47.97 < M_\infty < 48.77$
F4 + PLGA	$0.093 < k < 0.237$	$16.21 < M_t < 27.68$	$48.1 < M_\infty < 48.65$

<sup>a</sup> $K$ ,  $M_t$ , and  $M_\infty$  are represented by a range of values, reflecting the diverse coefficients observed in each of the 16 distinct sections analyzed for every formulation.

from a polymeric system characterized by the presence of different polymers. Figure 9A–D seems to exhibit a multiphase drug release pattern, which is typical for composite materials like the blends used in this study. After the initial burst, the release reaches a steady state, possibly due to the diffusion-controlled mechanism becoming dominant or a balance achieved between drug diffusion and matrix erosion. Using the Korsmeyer–Peppas model, the calculated values of the regression coefficients (R<sup>2</sup>) ranged from 0.9714 to 0.9882 across all evaluated sections.

Table 2 presents the mathematical parameters derived from the general equation  $\frac{M_t}{M_\infty} = 1 - e^{-kt^n}$ , where  $M_t$  is the amount of drug released at time  $t$ ,  $M_\infty$  is the total amount of drug in the system,  $k$  is the rate constant, and  $n$  is the release exponent for each section. These findings are in accordance with the typical release mechanism first identified by Korsmeyer for polymeric systems.<sup>109</sup>

We detected a release of drug mostly from the central sections, while the peripheral sections play a marginal role,

which is consistent with what we observed for the nanofiber mats without a PLGA layer. We demonstrated that with additional manufacturing steps, we can tune and extend the release profile of VAN for up to 7 days. We can speculate that additional iterations of the same process could extend even further in time for the release of VAN in future applications. It is worth noting that the PLGA coating proved beneficial in slowing down the release of VAN, allowing us to achieve a sustained release for up to 7 days. However, the overall efficiency decreased when compared to the coating obtained without the additional PLGA layer. This is because PLGA retained VAN from being released.<sup>110,111</sup> To counteract this decrease in release efficiency, increasing the VAN content in the electrospinning solution could match the release observed in the coatings without the additional PLGA layer. More in detail, after 3 h, F2 and F4 had a release ranging from 88 to 95%, while F2 and F4 with PLGA coating had a release ranging from 44 to 72%. To increase efficiency, it could be sufficient to increase the VAN content of F2 and F4 + PLGA by at least

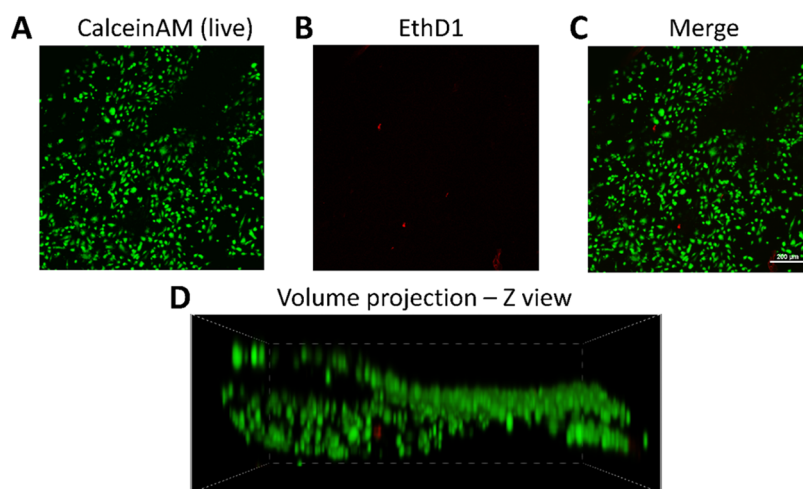


**Figure 10.** Human umbilical vein endothelial cells (HUVECs) seeded onto the CNC. High viability was observed after 24 h for both formulations F2 and F4. Panel (C) shows an abundance of live cells (stained with CalceinAM+) (A) and low levels of cell death (stained with ethidium homodimer+) (B) in Z-stack images of cells taken at the patch surface from formulation F2. Volume projection demonstrates the attachment of HUVEC cells across the surface of the patch obtained from formulation F4 (D).

40% to achieve a comparable release efficiency for both fast- and slow-release coatings.

Our developed coating could be applied to various implantable devices, particularly those with a high risk of device-related infections, such as vascular grafts. Ensuring proper adhesion of the coating to the vascular graft is crucial for its durability and prevention of premature detachment from prosthetic vascular grafts. Two possible approaches have been identified so far and are currently being tested by our group. These methods include chemical wet etching and plasma etching in combination with a gelatin coating of the outer layer of the prosthetic vascular graft. Regarding chemical wet etching, a growing body of research highlights its efficacy in improving the adhesive properties of PTFE and PET substrates.<sup>112,113</sup> Since many prosthetic vascular grafts are constructed from these materials, this technique emerges as a promising option for surface modification to augment the adhesiveness of the outer layer, facilitating the grafting of our coating.

Plasma etching also presents itself as a potential avenue.<sup>114,115</sup> However, considering the temporary nature of the increased adhesiveness achieved through it, this approach might be implemented in conjunction with a gelatin coating to establish a more durable effect. Gelatin exhibits unique properties: at 60 °C, it behaves like a liquid, while at temperatures below 40 °C, it solidifies, displaying a sticky behavior. Numerous instances of its application as a “natural glue” have been documented in the literature.<sup>116,117</sup> Moreover, gelatin with its intrinsic biocompatibility properties could enhance the overall biocompatibility of the prosthetic vascular graft, improving cell attachment.<sup>118,119</sup>

Implantable devices are particularly suitable for providing long-term antibiotic therapy. In chronic infections or conditions requiring prolonged treatment, such as osteomyelitis or device-related infections (VGI), implantable devices offer a reliable and sustained drug delivery solution.<sup>120–122</sup> They eliminate the need for frequent administration or hospital visits, thereby enhancing patient convenience and reducing healthcare costs. By delivering antibiotics directly to the affected area, the concentration of the drug at the site can be significantly higher than systemic administration.<sup>123,124</sup> This

localized approach helps to increase drug efficacy while reducing the risk of systemic side effects. Furthermore, local antibiotic delivery may reduce the risk of developing antibiotic resistance. By delivering antibiotics directly to the infection site, suboptimal drug concentrations that can promote the emergence of resistant strains are avoided.<sup>125,126</sup> Finally, sustained exposure to antibiotics through local delivery can enhance the effectiveness of the treatment, reducing the likelihood that resistant bacterial populations survive and proliferate.

**Biocompatibility Assessment.** HUVECs, or human umbilical vein endothelial cells, have been extensively studied for their biocompatibility and potential use in the endothelialization of vascular grafts.<sup>127</sup> For this reason, we decided to assess the biocompatibility of the final construct with HUVEC cells. After seeding HUVECs onto the nanofibrous mats of F2 and F4 with an additional PLGA coating, we evaluated their viability following 24 h of incubation. Figure 10 shows an abundance of live cells (stained with CalceinAM+) and low levels of cell death (stained with ethidium homodimer+) in Z-stack images of cells taken at the patch’s surface. The volume projection in Figure 10 demonstrates the attachment of HUVEC cells across the patch’s surface. Endothelialization refers to the process of forming a functional endothelial cell layer on the luminal surface of an implanted vascular graft, which can help improve the long-term patency and biocompatibility of the graft.<sup>128</sup> The properties of the nanofibrous mat play a critical role in endothelialization. Factors such as the material composition, surface topography, and mechanical properties of the material can affect cell adhesion, migration, and proliferation. If the mat does not provide a suitable environment for endothelial cell growth and function, it can hinder the endothelialization process.<sup>129</sup>

## CONCLUSIONS

In this study, we developed several iterations of polymeric solutions to obtain a chitosan-based, drug-eluting nanofibrous coating for vascular grafts. Blends combining chitosan with PVA or PEO exhibited superior electrospinnability compared to that of chitosan alone. Several blends were investigated, and rheological characterization was fundamental in the selection

process. Two different VAN concentrations, namely, 1 and 10 mg/mL, were evaluated to assess how different payloads could affect the electrospinning process. A successful nanofibrous deposition was obtained with both PVA and PEO containing the highest VAN content. The nanofibrous coatings obtained from the electrospinning of these formulations, F2 and F4, were characterized by means of TGA and FT-IR to verify the presence of VAN. Direct quantification of VAN released over time was assessed through HPLC analysis. Interestingly, VAN was released in less than 24 h; therefore, to slow down the release kinetics and have a longer elution, a PLGA layer was electrospun on top of the nanofibrous mats obtained with formulations F2 and F4. Subsequent quantitative analysis showed that the addition of a PLGA layer effectively slowed the release kinetics. VAN was released for up to 7 days. Following the analytical evaluation, the biocompatibility assessment revealed the high viability of HUVEC cells seeded on the nanofibrous mats. The results obtained provide an exciting preclinical proof-of-concept, as well as a strong scientific foundation toward further clinical development of a nanofibrous drug-eluting coating of vascular grafts for the treatment of VGIs. In conclusion, the elution of antibiotics from VGs provides targeted delivery, sustained release, higher local drug concentrations, reduced systemic exposure, potential for increased drug doses, biofilm prevention, and options for combination therapy. These advantages make systems like the one proposed an attractive strategy for managing VGIs, improving treatment efficacy, and reducing the risk of complications.

## ■ ASSOCIATED CONTENT

### SI Supporting Information

The Supporting Information is available free of charge at <https://pubs.acs.org/doi/10.1021/acsomega.3c08113>.

The Cox–Merz relationship for all 4 formulations (Figure S1); heat maps of the released VAN from the nanofibrous mats obtained with formulations F1 and F3 (Figure S2); direct quantification with HPLC of the release kinetics from the drug-eluting nanofibrous mats obtained with formulations F1 and F3 (Figure S3); and microscopic characterization of the PLGA nanofibrous coating electrospun on the CNC mats (Figure S4) (PDF)

## ■ AUTHOR INFORMATION

### Corresponding Author

**Francesca Taraballi** – *Center for Musculoskeletal Regeneration, Houston Methodist Academic Institute, Houston, Texas 77030-2707, United States; Department of Orthopedics and Sport Medicine, Houston Methodist Hospital, Houston, Texas 77030-2707, United States;* [orcid.org/0000-0002-4959-1169](https://orcid.org/0000-0002-4959-1169); Email: [ftaraballi2@houstonmethodist.org](mailto:ftaraballi2@houstonmethodist.org)

### Authors

**Stefano Serpelloni** – *Center for Musculoskeletal Regeneration, Houston Methodist Academic Institute, Houston, Texas 77030-2707, United States; Department of Electronics, Information and Bioengineering (DEIB), Politecnico di Milano 20133, Italy; Department of Orthopedics and Sport Medicine, Houston Methodist Hospital, Houston, Texas 77030-2707, United States*

**Michael Ellis Williams** – *Center for Musculoskeletal Regeneration, Houston Methodist Academic Institute, Houston, Texas 77030-2707, United States; Reproductive Biology and Gynaecological Oncology Group, Swansea University Medical School, Swansea SA2 8QA, U.K.*

**Sergio Caserta** – *Department of Chemical Materials and Industrial Production Engineering, University of Naples Federico II, Naples 80138, Italy;* [orcid.org/0000-0002-4400-0059](https://orcid.org/0000-0002-4400-0059)

**Shashank Sharma** – *Department of Cardiovascular Surgery, Houston Methodist Hospital, Houston, Texas 77030-2707, United States*

**Maham Rahimi** – *Department of Cardiovascular Surgery, Houston Methodist Hospital, Houston, Texas 77030-2707, United States*

Complete contact information is available at:

<https://pubs.acs.org/10.1021/acsomega.3c08113>

## ■ Funding

This work was supported by the George and Angelina Kostas Research Center for Cardiovascular Nanomedicine.

## ■ Notes

The authors declare no competing financial interest.

## ■ ACKNOWLEDGMENTS

The authors would like to thank Amanda Weiskoff, Ph.D. (Academic Affairs, Houston Methodist Academic Institute), for scientific editing assistance.

## ■ REFERENCES

- (1) Nations, U. World population prospects 2019. *Vol Department of Economic Social Affairs: Population Division*, 2019.
- (2) Heron, M. P., Deaths: leading causes for 2016. 2018.
- (3) Lakatta, E. G.; Levy, D. Arterial and cardiac aging: major shareholders in cardiovascular disease enterprises: Part I: aging arteries: a “set up” for vascular disease. *Circulation* **2003**, *107* (1), 139–146.
- (4) Donato, A. J.; Machin, D. R.; Lesniewski, L. A. Mechanisms of Dysfunction in the Aging Vasculature and Role in Age-Related Disease. *Circ. Res.* **2018**, *123* (7), 825–848.
- (5) Said, M. A.; Eppinga, R. N.; Lipsic, E.; Verweij, N.; van der Harst, P. Relationship of Arterial Stiffness Index and Pulse Pressure With Cardiovascular Disease and Mortality. *J. Am. Heart Assoc.* **2018**, *7* (2), No. e007621, DOI: [10.1161/JAHA.117.007621](https://doi.org/10.1161/JAHA.117.007621).
- (6) Criqui, M. H.; Matsushita, K.; Aboyans, V.; Hess, C. N.; Hicks, C. W.; Kwan, T. W.; McDermott, M. M.; Misra, S.; Ujueta, F.; American Heart Association Council on Epidemiology and Prevention; Council on Arteriosclerosis, Thrombosis and Vascular Biology; Council on Cardiovascular Radiology and Intervention; Council on Lifestyle and Cardiometabolic Health; Council on Peripheral Vascular Disease; and Stroke Council. Lower Extremity Peripheral Artery Disease: Contemporary Epidemiology, Management Gaps, and Future Directions: A Scientific Statement From the American Heart Association. *Circulation* **2021**, *144* (9), e171–e191, DOI: [10.1161/CIR.0000000000001005](https://doi.org/10.1161/CIR.0000000000001005).
- (7) Morley, R. L.; Sharma, A.; Horsch, A. D.; Hinchliffe, R. J. Peripheral artery disease. *BMJ* **2018**, *360*, No. j5842, DOI: [10.1136/bmj.j5842](https://doi.org/10.1136/bmj.j5842).
- (8) Forman, D. E.; Maurer, M. S.; Boyd, C.; Brindis, R.; Salive, M. E.; Horne, F. M.; Bell, S. P.; Fulmer, T.; Reuben, D. B.; Zieman, S.; Rich, M. W. Multimorbidity in Older Adults With Cardiovascular Disease. *J. Am. Coll. Cardiol.* **2018**, *71* (19), 2149–2161.
- (9) Anagnostopoulos, A.; Ledergerber, B.; Kuster, S. P.; Scherrer, A. U.; Naf, B.; Greiner, M. A.; Rancic, Z.; Kobe, A.; Bettex, D.; Hasse, B.; Study, V. C.; et al. Inadequate Perioperative Prophylaxis and

- Postsurgical Complications After Graft Implantation Are Important Risk Factors for Subsequent Vascular Graft Infections: Prospective Results From the Vascular Graft Infection Cohort Study. *Clin. Infect. Dis.* **2019**, *69* (4), 621–630.
- (10) Mufty, H.; Van den Bergh, M.; Meuris, B.; Metsemakers, W. J.; Fourneau, I. Clinical Studies Reporting on Vascular Graft Coatings for the Prevention of Aortic Graft Infection: A Systematic Review and Meta-Analysis. *Eur. J. Vasc. Endovasc. Surg.* **2022**, *63* (1), 112–118.
- (11) Koc, C.; Akbulut, S.; Ozdemir, F.; Kose, A.; Isik, B.; Yologlu, S.; Yilmaz, S. Analysis of risk factors affecting the development of infection in artificial vascular grafts used for reconstruction of middle hepatic vein tributaries in living donor liver transplantation. *Transplantation* **2019**, *103* (9), 1871–1876.
- (12) Rubalskii, E.; Ruenke, S.; Salmoukas, C.; Boyle, E. C.; Warnecke, G.; Tudorache, I.; Shrestha, M.; Schmitto, J. D.; Martens, A.; Rojas, S. V.; Ziesing, S.; Bochkareva, S.; Kuehn, C.; Haverich, A. Bacteriophage Therapy for Critical Infections Related to Cardiothoracic Surgery. *Antibiotics* **2020**, *9* (5), 232.
- (13) Hasse, B.; Husmann, L.; Zinkernagel, A.; Weber, R.; Lachat, M.; Mayer, D. Vascular graft infections. *Swiss Med. Wkly* **2013**, *143* (0304), w13754.
- (14) Revest, M.; Camou, F.; Senneville, E.; Caillon, J.; Laurent, F.; Calvet, B.; Feugier, P.; Batt, M.; Chidiac, C.; Groupe de Réflexion sur les Infections de Prothèses vasculaires (GRIP). Medical treatment of prosthetic vascular graft infections: Review of the literature and proposals of a Working Group. *Int. J. Antimicrob. Agents* **2015**, *46* (3), 254–265, DOI: 10.1016/j.ijantimicag.2015.04.014.
- (15) Legout, L.; Sarraz-Bournet, B.; D'Elia, P. V.; Devos, P.; Pasquet, A.; Caillaux, M.; Wallet, F.; Yazdanpanah, Y.; Senneville, E.; Haulon, S.; Leroy, O. Characteristics and prognosis in patients with prosthetic vascular graft infection: a prospective observational cohort study. *Clin. Microbiol. Infect.* **2012**, *18* (4), 352–358.
- (16) Erb, S.; Sidler, J. A.; Elzi, L.; Gurke, L.; Battegay, M.; Widmer, A. F.; Weisser, M. Surgical and antimicrobial treatment of prosthetic vascular graft infections at different surgical sites: a retrospective study of treatment outcomes. *PLoS One* **2014**, *9* (11), No. e112947, DOI: 10.1371/journal.pone.0112947.
- (17) Wilson, W. R.; Bower, T. C.; Creager, M. A.; Amin-Hanjani, S.; O'Gara, P. T.; Lockhart, P. B.; Darouiche, R. O.; Ramlawi, B.; Derdeyn, C. P.; Bolger, A. F.; Levison, M. E.; Taubert, K. A.; Baltimore, R. S.; Baddour, L. M.; American Heart Association Committee on Rheumatic Fever, Endocarditis, and Kawasaki Disease of the Council on Cardiovascular Disease in the Young; Council on Cardiovascular and Stroke Nursing; Council on Cardiovascular Radiology and Intervention; Council on Cardiovascular Surgery and Anesthesia; Council on Peripheral Vascular Disease; and Stroke Council. Vascular Graft Infections, Mycotic Aneurysms, and Endovascular Infections: A Scientific Statement From the American Heart Association. *Circulation* **2016**, *134* (20), e412–e460, DOI: 10.1161/CIR.0000000000000457.
- (18) Sousa, J. V.; Antunes, L.; Mendes, C.; Marinho, A.; Gonçalves, A.; Gonçalves, O.; Matos, A. Prosthetic vascular graft infections: a center experience. *J. Angiology Cir. Vasc.* **2014**, *10* (2), 52–57.
- (19) Post, I. C.; Vos, C. G. Systematic Review and Meta-Analysis on the Management of Open Abdominal Aortic Graft Infections. *Eur. J. Vasc. Endovasc. Surg.* **2019**, *58* (2), 258–281.
- (20) Töpel, I.; Audebert, F.; Betz, T.; Steinbauer, M. G. Microbial spectrum and primary resistance to rifampicin in infectious complications in vascular surgery: limits to the use of rifampicin-bonded prosthetic grafts. *Angiology* **2010**, *61* (5), 423–426.
- (21) Lin, Z.; Wu, T.; Wang, W.; Li, B.; Wang, M.; Chen, L.; Xia, H.; Zhang, T. J. Biofunctions of antimicrobial peptide-conjugated alginate/hyaluronic acid/collagen wound dressings promote wound healing of a mixed-bacteria-infected wound. *Int. J. Biol. Macromol.* **2019**, *140*, 330–342, DOI: 10.1016/j.ijbiomac.2019.08.087.
- (22) López-Jácome, E.; Franco-Cendejas, R.; Quezada, H.; Morales-Espinosa, R.; Castillo-Juárez, I.; González-Pedrajo, B.; Fernández-Presas, A. M.; Tovar-García, A.; Angarita-Zapata, V.; Licona-Limón, P. The race between drug introduction and appearance of microbial resistance. *Curr. Opin. Pharmacol.* **2019**, *48*, 48–56.
- (23) Ibrahim, D.; Jabbour, J. F.; Kanj, S. S. Current choices of antibiotic treatment for Pseudomonas aeruginosa infections. *Curr. Opin. Infect. Dis.* **2020**, *33* (6), 464–473.
- (24) Fayol, D.; Le Visage, C.; Ino, J.; Gazeau, F.; Letourneur, D.; Wilhelm, C. Design of biomimetic vascular grafts with magnetic endothelial patterning. *Cell Transplant.* **2013**, *22* (11), 2105–2118.
- (25) Shin, H.; Jo, S.; Mikos, A. G. Biomimetic materials for tissue engineering. *Biomaterials* **2003**, *24* (24), 4353–4364.
- (26) Jia, W.; Li, M.; Weng, H.; Gu, G.; Chen, Z. Design and comprehensive assessment of a biomimetic tri-layer tubular scaffold via biodegradable polymers for vascular tissue engineering applications. *Mater. Sci. Eng., C* **2020**, *110*, 110717.
- (27) Shi, J.; Zhang, X.; Jiang, L.; Zhang, L.; Dong, Y.; Midgley, A. C.; Kong, D.; Wang, S. Regulation of the inflammatory response by vascular grafts modified with Aspirin-Triggered Resolvin D1 promotes blood vessel regeneration. *Acta Biomater.* **2019**, *97*, 360–373.
- (28) Zhuang, Y.; Zhang, C.; Cheng, M.; Huang, J.; Liu, Q.; Yuan, G.; Lin, K.; Yu, H. Challenges and strategies for in situ endothelialization and long-term lumen patency of vascular grafts. *Bioact. Mater.* **2021**, *6* (6), 1791–1809.
- (29) Zhou, J.; Wang, M.; Wei, T.; Bai, L.; Zhao, J.; Wang, K.; Feng, Y. Endothelial Cell-Mediated Gene Delivery for In Situ Accelerated Endothelialization of a Vascular Graft. *ACS Appl. Mater. Interfaces* **2021**, *13* (14), 16097–16105.
- (30) Luo, J.; Qin, L.; Zhao, L.; Gui, L.; Ellis, M. W.; Huang, Y.; Kural, M. H.; Clark, J. A.; Ono, S.; Wang, J.; Yuan, Y.; Zhang, S. M.; Cong, X.; Li, G.; Riaz, M.; Lopez, C.; Hotta, A.; Campbell, S.; Tellides, G.; Dardik, A.; Niklason, L. E.; Qyang, Y. Tissue-Engineered Vascular Grafts with Advanced Mechanical Strength from Human iPSCs. *Cell Stem Cell* **2020**, *26* (2), 251–261 e8.
- (31) Leal, B. B. J.; Wakabayashi, N.; Oyama, K.; Kamiya, H.; Braghioroli, D. I.; Pranke, P. Vascular Tissue Engineering: Polymers and Methodologies for Small Caliber Vascular Grafts. *Front. Cardiovasc. Med.* **2020**, *7*, No. 592361.
- (32) Zhao, L.; Li, X.; Yang, L.; Sun, L.; Mu, S.; Zong, H.; Li, Q.; Wang, F.; Song, S.; Yang, C.; Zhao, C.; Chen, H.; Zhang, R.; Wang, S.; Dong, Y.; Zhang, Q. Evaluation of remodeling and regeneration of electrospun PCL/fibrin vascular grafts in vivo. *Mater. Sci. Eng., C* **2021**, *118*, No. 111441.
- (33) Zavan, B.; Gardin, C.; Guarino, V.; Rocca, T.; Cruz Maya, I.; Zanotti, F.; Ferroni, L.; Brunello, G.; Chachques, J. C.; Ambrosio, L.; Gasbarro, V. Electrospun PCL-Based Vascular Grafts: In Vitro Tests. *Nanomaterials* **2021**, *11* (3), 751.
- (34) Zhu, T.; Gu, H.; Zhang, H.; Wang, H.; Xia, H.; Mo, X.; Wu, J. Covalent grafting of PEG and heparin improves biological performance of electrospun vascular grafts for carotid artery replacement. *Acta Biomater.* **2021**, *119*, 211–224.
- (35) Martău, G. A.; Mihai, M.; Vodnar, D. The use of chitosan, alginate, and pectin in the biomedical and food sector-biocompatibility, bioadhesiveness, and biodegradability. *Polymers* **2019**, *11* (11), No. 1837, DOI: 10.3390/polym11111837.
- (36) Parhi, R. Drug delivery applications of chitin and chitosan: a review. *Review* **2020**, *18* (3), 577–594, DOI: 10.1007/s10311-020-00963-5.
- (37) Mohebbi, S.; Nezhad, M. N.; Zarrintaj, P.; Jafari, S. H.; Gholizadeh, S. S.; Saeb, M. R.; Mozafari, M. Chitosan in Biomedical Engineering: A Critical Review. *Curr. Stem Cell Res. Ther.* **2019**, *14* (2), 93–116.
- (38) Peers, S.; Montebault, A.; Ladaviere, C. Chitosan hydrogels for sustained drug delivery. *J. Controlled Release* **2020**, *326*, 150–163.
- (39) Cataldo, M. A.; Tacconelli, E.; Grilli, E.; Pea, F.; Petrosillo, N. Continuous versus intermittent infusion of vancomycin for the treatment of Gram-positive infections: systematic review and meta-analysis. *J. Antimicrob. Chemother.* **2012**, *67* (1), 17–24.
- (40) Bloem, A.; Bax, H. I.; Yusuf, E.; Verkaik, N. J. New-Generation Antibiotics for Treatment of Gram-Positive Infections: A Review with

- Focus on Endocarditis and Osteomyelitis. *J. Clin. Med.* **2021**, *10* (8), 1743.
- (41) Tao, J.; Zhang, Y.; Shen, A.; Yang, Y.; Diao, L.; Wang, L.; Cai, D.; Hu, Y. Injectable Chitosan-Based Thermosensitive Hydrogel/Nanoparticle-Loaded System for Local Delivery of Vancomycin in the Treatment of Osteomyelitis. *Int. J. Nanomedicine* **2020**, *15*, 5855–5871.
- (42) Hwang, J.; Huang, H.; Sullivan, M. O.; Kiick, K. L. Controlled Delivery of Vancomycin from Collagen-tethered Peptide Vehicles for the Treatment of Wound Infections. *Mol. Pharmaceutics* **2023**, *20* (3), 1696–1708.
- (43) Krishnan, A. G.; Biswas, R.; Menon, D.; Nair, M. B. Biodegradable nanocomposite fibrous scaffold mediated local delivery of vancomycin for the treatment of MRSA infected experimental osteomyelitis. *Biomater Sci.* **2020**, *8* (9), 2653–2665.
- (44) Koosha, M.; Mirzadeh, H. Electrospinning, mechanical properties, and cell behavior study of chitosan/PVA nanofibers. *J. Biomed. Mater. Res.* **2015**, *103* (9), 3081–3093.
- (45) Mata, G. C. D.; Morais, M. S.; Oliveira, W. P.; Aguiar, M. L. Composition Effects on the Morphology of PVA/Chitosan Electrospun Nanofibers. *Polymers* **2022**, *14* (22), 4856.
- (46) Mengistu Lemma, S.; Bossard, F.; Rinaudo, M. Preparation of Pure and Stable Chitosan Nanofibers by Electrospinning in the Presence of Poly(ethylene oxide). *Int. J. Mol. Sci.* **2016**, *17* (11), No. 1790.
- (47) Kuntzler, S. G.; Costa, J. A. V.; Morais, M. G. Development of electrospun nanofibers containing chitosan/PEO blend and phenolic compounds with antibacterial activity. *Int. J. Biol. Macromol.* **2018**, *117*, 800–806.
- (48) Yuan, Y.; Lee, T. R. Contact angle and wetting properties. In *Surface Science Techniques*; Springer, 2013; pp 3–34.
- (49) Usman, M.; Hempel, G. Development and validation of an HPLC method for the determination of vancomycin in human plasma and its comparison with an immunoassay (PETINIA). *Springerplus* **2016**, *5*, No. 124.
- (50) Ke, C. L.; Deng, F. S.; Chuang, C. Y.; Lin, C. H. Antimicrobial Actions and Applications of Chitosan. *Polymers* **2021**, *13* (6), 904.
- (51) Moeini, A.; Pedram, P.; Makvandi, P.; Malinconico, M.; Gomez d'Ayala, G. Wound healing and antimicrobial effect of active secondary metabolites in chitosan-based wound dressings: A review. *Carbohydr. Polym.* **2020**, *233*, No. 115839.
- (52) Rashki, S.; Asgarpour, K.; Tarrahimofrad, H.; Hashemipour, M.; Ebrahimi, M. S.; Fathizadeh, H.; Khorshidi, A.; Khan, H.; Marzhooseyni, Z.; Salavati-Niasari, M.; Mirzaei, H. Chitosan-based nanoparticles against bacterial infections. *Carbohydr. Polym.* **2021**, *251*, No. 117108.
- (53) Valachová, K.; El Meligy, M. A.; Soltes, L. Hyaluronic acid and chitosan-based electrospun wound dressings: Problems and solutions. *Int. J. Biol. Macromol.* **2022**, *206*, 74–91.
- (54) Rezaei, F. S.; Sharifianjazi, F.; Esmailkhanian, A.; Salehi, E. Chitosan films and scaffolds for regenerative medicine applications: A review. *Carbohydr. Polym.* **2021**, *273*, No. 118631.
- (55) Wu, J. Y.; Wang, C. Y.; Chen, K. H.; Lai, Y. R.; Chiu, C. Y.; Lee, H. C.; Chang, Y. K. Electrospinning of Quaternized Chitosan-Poly(vinyl alcohol) Composite Nanofiber Membrane: Processing Optimization and Antibacterial Efficacy. *Membranes* **2022**, *12* (3), 332.
- (56) Sapkota, S.; Chou, S. F. Electrospun Chitosan-based Fibers for Wound Healing Applications. *J. Biomater.* **2020**, *4* (2), 51–57.
- (57) Amiri, N.; Ajami, S.; Shahroodi, A.; Jannatabadi, N.; Darban, S. A.; Bazzaz, B. S. F.; Pishavar, E.; Kalalinia, F.; Movaffagh, J. Teicoplanin-loaded chitosan-PEO nanofibers for local antibiotic delivery and wound healing. *Int. J. Biol. Macromol.* **2020**, *162*, 645–656.
- (58) Azimi, B.; Maleki, H.; Gigante, V.; Bagherzadeh, R.; Mezzetta, A.; Milazzo, M.; Guazzelli, L.; Cinelli, P.; Lazzeri, A.; Danti, S. Cellulose-based fiber spinning processes using ionic liquids. *Cellulose* **2022**, *29* (6), 3079–3129.
- (59) Pillai, C. K.; Paul, W.; Sharma, C. P. Chitin and chitosan polymers: Chemistry, solubility and fiber formation. *Prog. Polym. Sci.* **2009**, *34* (7), 641–678.
- (60) Geng, X.; Kwon, O. H.; Jang, J. Electrospinning of chitosan dissolved in concentrated acetic acid solution. *Biomaterials* **2005**, *26* (27), 5427–5432.
- (61) Liu, Y.; Chen, X.; Yu, D. G.; Liu, H.; Liu, Y.; Liu, P. Electrospun PVP-Core/PHBV-Shell Fibers to Eliminate Tailing Off for an Improved Sustained Release of Curcumin. *Mol. Pharmaceutics* **2021**, *18* (11), 4170–4178.
- (62) Zeng, J.; Yang, L.; Liang, Q.; Zhang, X.; Guan, H.; Xu, X.; Chen, X.; Jing, X. Influence of the drug compatibility with polymer solution on the release kinetics of electrospun fiber formulation. *J. Controlled Release* **2005**, *105* (1–2), 43–51.
- (63) Verreck, G.; Chun, I.; Peeters, J.; Rosenblatt, J.; Brewster, M. E. Preparation and characterization of nanofibers containing amorphous drug dispersions generated by electrostatic spinning. *Pharm. Res.* **2003**, *20* (5), 810–817.
- (64) Wang, Y.; Wang, B.; Qiao, W.; Yin, T. A novel controlled release drug delivery system for multiple drugs based on electrospun nanofibers containing nanoparticles. *J. Pharm. Sci.* **2010**, *99* (12), 4805–4811.
- (65) Rybak, M.; Lomaestro, B.; Rotschafer, J. C.; Moellering, R., Jr.; Craig, W.; Billeter, M.; Dalovisio, J. R.; Levine, D. P. Therapeutic monitoring of vancomycin in adult patients: a consensus review of the American Society of Health-System Pharmacists, the Infectious Diseases Society of America, and the Society of Infectious Diseases Pharmacists. *Am. J. Health-Syst. Pharm.* **2009**, *66* (1), 82–98.
- (66) Zonozi, R.; Wu, A.; Shin, J.-I.; Secora, A.; Coresh, J.; Inker, L. A.; Chang, A. R.; Grams, M. E. *Elevated Vancomycin Trough Levels in a Tertiary Health System: Frequency, Risk Factors, and Prognosis*, Mayo Clinic Proceedings; Elsevier, 2019; pp 17–26.
- (67) Sousa, J. V.; Antunes, L.; Mendes, C.; Marinho, A.; Gonçalves, A.; Gonçalves, Ó.; Matos, A. Prosthetic vascular graft infections: a center experience. *Angiologia Cir. Vasc.* **2014**, *10* (2), 52–57.
- (68) Patel, S.; Preuss, C. V.; Bernice, F. Vancomycin. In *StatPearls*; StatPearls Publishing: Treasure Island (FL), March 24, 2023. <https://www.ncbi.nlm.nih.gov/books/NBK459263/>.
- (69) Rybak, M. J.; Le, J.; Lodise, T. P.; Levine, D. P.; Bradley, J. S.; Liu, C.; Mueller, B. A.; Pai, M. P.; Wong-Beringer, A.; Rotschafer, J. C.; Rodvold, K. A.; Maples, H. D.; Lomaestro, B. M. Therapeutic monitoring of vancomycin for serious methicillin-resistant *Staphylococcus aureus* infections: A revised consensus guideline and review by the American Society of Health-System Pharmacists, the Infectious Diseases Society of America, the Pediatric Infectious Diseases Society, and the Society of Infectious Diseases Pharmacists. *Am. J. Health-Syst. Pharm.* **2020**, *77* (11), 835–864.
- (70) Zamoner, W.; Prado, I. R. S.; Balbi, A. L.; Ponce, D. Vancomycin dosing, monitoring and toxicity: Critical review of the clinical practice. *Clin. Exp. Pharmacol. Physiol.* **2019**, *46* (4), 292–301.
- (71) Naendrup, J. H.; Marche, B.; de Sa, D.; Koenen, P.; Otchwemah, R.; Wafaisade, A.; Pfeiffer, T. R. Vancomycin-soaking of the graft reduces the incidence of septic arthritis following ACL reconstruction: results of a systematic review and meta-analysis. *Knee Surg. Sports Traumatol. Arthrosc.* **2020**, *28* (4), 1005–1013.
- (72) Harper, K. D.; Park, K. J.; Brozovich, A. A.; Sullivan, T. C.; Serpelloni, S.; Taraballi, F.; Incavo, S. J.; Clyburn, T. A. Otto Auftranc Award: Intraosseous Vancomycin in Total Hip Arthroplasty—Superior Tissue Concentrations and Improved Efficiency. *J. Arthroplasty* **2023**, *38* (7), S11–S15.
- (73) Carroll, C. P.; Joo, Y. L. Electrospinning of viscoelastic Boger fluids: Modeling and experiments. *Phys. Fluids* **2006**, *18* (5), No. 053102, DOI: 10.1063/1.2200152.
- (74) Dodero, A.; Vicini, S.; Alloisio, M.; Castellano, M. Sodium alginate solutions: Correlation between rheological properties and spinnability. *J. Mater. Sci.* **2019**, *54* (10), 8034–8046.
- (75) Qin, X. H.; Yang, E. L.; Li, N.; Wang, S. Y. Effect of different salts on electrospinning of polyacrylonitrile (PAN) polymer solution. *Appl. Polym.* **2007**, *103* (6), 3865–3870, DOI: 10.1002/app.25498.

- (76) Tiwari, S. K.; Venkatraman, S. S. Importance of viscosity parameters in electrospinning: Of monolithic and core-shell fibers. *J. Mater. Sci. Eng. C* **2012**, *32* (5), 1037–1042.
- (77) Klossner, R. R.; Queen, H. A.; Coughlin, A. J.; Krause, W. E. Correlation of chitosan's rheological properties and its ability to electrospin. *Biomacromolecules* **2008**, *9* (10), 2947–2953.
- (78) Li, Z.; Wang, C.; Li, Z.; Wang, C. Effects of Working Parameters on Electrospinning. *One-Dimens. Nanostruct.* **2013**, 15–28.
- (79) Sun, J.; Perry, S. L.; Schiffman, J. D. Electrospinning Nanofibers from Chitosan/Hyaluronic Acid Complex Coacervates. *Biomacromolecules* **2019**, *20* (11), 4191–4198.
- (80) Pakravan, M.; Heuzey, M.-C.; Ajji, A. A fundamental study of chitosan/PEO electrospinning. *Polymers* **2011**, *52* (21), 4813–4824.
- (81) Li, Z.; Lei, I. M.; Davoodi, P.; Huleihel, L.; Huang, Y. Y. S. Solution Formulation and Rheology for Fabricating Extracellular Matrix-Derived Fibers Using Low-Voltage Electrospinning Patterning. *ACS Biomater. Sci. Eng.* **2019**, *5* (7), 3676–3684.
- (82) Viola, G.; Chang, J.; Maltby, T.; Steckler, F.; Jomaa, M.; Sun, J.; Edusei, J.; Zhang, D.; Vilches, A.; Gao, S.; Liu, X.; Saeed, S.; Zabalawi, H.; Gale, J.; Song, W. Bioinspired Multiresonant Acoustic Devices Based on Electrospun Piezoelectric Polymeric Nanofibers. *ACS Appl. Mater. Interfaces* **2020**, *12* (31), 34643–34657.
- (83) Carranza, T.; Uranga, J.; Irastorza, A.; Izeta, A.; Guerrero, P.; de la Caba, K. Combination of 3D printing and electrospinning to develop chitin/gelatin/PVA scaffolds. *Int. J. Bioprint.* **2023**, *9* (3), No. 701, DOI: 10.18063/ijb.701.
- (84) Gupta, D.; Jassal, M.; Agrawal, A. K. The electrospinning behavior of poly (vinyl alcohol) in DMSO–water binary solvent mixtures. *RSC Adv.* **2016**, *6* (105), 102947–102955.
- (85) Sang, Z.; Zhang, W.; Zhou, Z.; Fu, H.; Tan, Y.; Sui, K.; Xia, Y. Functionalized alginate with liquid-like behaviors and its application in wet-spinning. *Carbohydr. Polym.* **2017**, *174*, 933–940.
- (86) Luo, H.; Xiao, Z.; Chen, Y.; Niu, Y.; Li, G. Phase separation kinetics and rheological behavior of Poly (ethylene oxide)/ionic liquid mixtures with large dynamic asymmetry. *Polymers* **2017**, *123*, 290–300.
- (87) Kumar, P.; Maiti, U. N.; Lee, K. E.; Kim, S. O. Rheological properties of graphene oxide liquid crystal. *Carbon* **2014**, *80*, 453–461.
- (88) Sivan, M.; Madheswaran, D.; Valtera, J.; Kostakova, E. K.; Lukas, D. Alternating current electrospinning: The impacts of various high-voltage signal shapes and frequencies on the spinnability and productivity of polycaprolactone nanofibers. *Mater. Des.* **2022**, *213*, No. 110308.
- (89) Sivan, M.; Madheswaran, D.; Hauzerova, S.; Novotny, V.; Hedvicakova, V.; Jencova, V.; Kostakova, E.; Schindler, M.; Lukas, D. AC electrospinning: Impact of high voltage and solvent on the electrospinnability and productivity of polycaprolactone electrospun nanofibrous scaffolds. *Mater. Today Chem.* **2022**, *26*, No. 101025.
- (90) Huang, Z.-M.; Zhang, Y.-Z.; Kotaki, M.; Ramakrishna, S. A review on polymer nanofibers by electrospinning and their applications in nanocomposites. *Compos. Sci. Technol.* **2003**, *63* (15), 2223–2253.
- (91) Hasan, A.; Memic, A.; Annabi, N.; Hossain, M.; Paul, A.; Dokmeci, M. R.; Dehghani, F.; Khademhosseini, A. Electrospun scaffolds for tissue engineering of vascular grafts. *Acta Biomater.* **2014**, *10* (1), 11–25.
- (92) Pakravan, M.; Heuzey, M.-C.; Ajji, A. A fundamental study of chitosan/PEO electrospinning. *Polymer* **2011**, *52* (21), 4813–4824.
- (93) Govindasamy, K.; Dahlan, N. A.; Janarthanan, P.; Goh, K. L.; Chai, S.-P.; Pasbakhsh, P. Electrospun chitosan/polyethylene-oxide (PEO)/halloysites (HAL) membranes for bone regeneration applications. *Appl. Clay Sci.* **2020**, *190*, No. 105601.
- (94) Hemmatian, T.; Lee, H.; Kim, J. Bacteria Adhesion of Textiles Influenced by Wettability and Pore Characteristics of Fibrous Substrates. *Polymers* **2021**, *13* (2), 223.
- (95) Li, W.; Thian, E. S.; Wang, M.; Wang, Z.; Ren, L. Surface Design for Antibacterial Materials: From Fundamentals to Advanced Strategies. *Adv. Sci.* **2021**, *8* (19), No. e2100368.
- (96) De-la-Pinta, I.; Cobos, M.; Ibarretxe, J.; Montoya, E.; Eraso, E.; Guraya, T.; Quindos, G. Effect of biomaterials hydrophobicity and roughness on biofilm development. *J. Mater. Sci. Mater. Med.* **2019**, *30* (7), No. 77.
- (97) Chen, Y.; Ding, Y.; Zheng, J. A polymer nanocomposite coating with enhanced hydrophilicity, antibacterial and antibiofouling properties: Role of polymerizable emulsifier/anionic ligand. *Chem. Eng. J.* **2020**, *379*, No. 122268.
- (98) Marra, D.; Karapantsios, T.; Caserta, S.; Secchi, E.; Holynska, M.; Labarthe, S.; Polizzi, B.; Ortega, S.; Kostoglou, M.; Lasseur, C.; Karapanagiotis, I.; Lecuyer, S.; Bridier, A.; Noiro-Gros, M. F.; Briandet, R. Migration of surface-associated microbial communities in spaceflight habitats. *Biofilm* **2023**, *5*, No. 100109.
- (99) Elbourne, A.; Chapman, J.; Gelmi, A.; Cozzolino, D.; Crawford, R. J.; Truong, V. K. Bacterial-nanostructure interactions: The role of cell elasticity and adhesion forces. *J. Colloid Interface Sci* **2019**, *546*, 192–210, DOI: 10.1016/j.jcis.2019.03.050.
- (100) Cheng, Y.; Feng, G.; Moraru, C. I. Micro- and Nanotopography Sensitive Bacterial Attachment Mechanisms: A Review. *Front. Microbiol.* **2019**, *10*, No. 191.
- (101) Zabiegaj, D.; Hajirasouliha, F.; Duilio, A.; Guido, S.; Caserta, S.; Kostoglou, M.; Petala, M.; Karapantsios, T.; Trybala, A. Wetting/spreading on porous media and on deformable, soluble structured substrates as a model system for studying the effect of morphology on biofilms wetting and for assessing anti-biofilm methods. *Curr. Opin. Colloid Interface Sci.* **2021**, *53*, No. 101426.
- (102) Jiang, J.; Liu, Y.; Chen, J.; Wang, X.; Yu, Z.; Li, W.; Zheng, G. In-situ molding of micro three-dimensional columnar structure by electric-field-focused electrospinning. *Mater. Today Commun.* **2023**, *35*, No. 105589.
- (103) Shi, R.; Tian, Y.; Wang, L. Bioinspired Fibers with Controlled Wettability: From Spinning to Application. *ACS Nano* **2021**, *15* (5), 7907–7930.
- (104) Suresh, S.; Becker, A.; Glasmacher, B. Impact of apparatus orientation and gravity in electrospinning—A review of empirical evidence. *Polymers* **2020**, *12* (11), 2448.
- (105) Li, Y.; Zhu, J.; Cheng, H.; Li, G.; Cho, H.; Jiang, M.; Gao, Q.; Zhang, X. Developments of advanced electrospinning techniques: A critical review. *Adv. Mater. Technol.* **2021**, *6* (11), No. 2100410.
- (106) Mancino, C.; Hendrickson, T.; Whitney, L. V.; Paradiso, F.; Abasi, S.; Tasciotti, E.; Taraballi, F.; Guiseppi-Elie, A. Electrospun electroconductive constructs of aligned fibers for cardiac tissue engineering. *Nanomedicine* **2022**, *44*, No. 102567.
- (107) Tsao, C. J.; Pandolfi, L.; Wang, X.; Minardi, S.; Lupo, C.; Evangelopoulos, M.; Hendrickson, T.; Shi, A.; Storci, G.; Taraballi, F.; Tasciotti, E. Electrospun Patch Functionalized with Nanoparticles Allows for Spatiotemporal Release of VEGF and PDGF-BB Promoting In Vivo Neovascularization. *ACS Appl. Mater. Interfaces* **2018**, *10* (51), 44344–44353.
- (108) Kormsmeier, R. W.; Von Meerwall, E.; Peppas, N. A. Solute and penetrant diffusion in swellable polymers. II. Verification of theoretical models. *J. Polym. Sci., Part B: Polym. Phys.* **1986**, *24* (2), 409–434.
- (109) Kormsmeier, R. W.; Gurny, R.; Doelker, E.; Buri, P.; Peppas, N. A. Mechanisms of solute release from porous hydrophilic polymers. *International journal of pharmaceutics* **1983**, *15* (1), 25–35.
- (110) Chen, D. W.; Hsu, Y.-H.; Liao, J.-Y.; Liu, S.-J.; Chen, J.-K.; Ueng, S. W.-N. Sustainable release of vancomycin, gentamicin and lidocaine from novel electrospun sandwich-structured PLGA/collagen nanofibrous membranes. *Int. J. Pharm.* **2012**, *430* (1–2), 335–341.
- (111) Jahanmard, F.; Croes, M.; Castilho, M.; Majed, A.; Steenbergen, M.; Lietaert, K.; Vogely, H.; Van Der Wal, B.; Stapels, D.; Malda, J.; et al. Bactericidal coating to prevent early and delayed implant-related infections. *J. Controlled Release* **2020**, *326*, 38–52.
- (112) Roina, Y.; Gonçalves, A. M.; Fregnaux, M.; Auber, F.; Herlem, G. Sodium naphthalenide diglyme solution for etching ptfte,

- characterizations and molecular modelization. *ChemistrySelect* **2022**, *7* (21), No. e202200153.
- (113) Badv, M.; Bayat, F.; Weitz, J. I.; Didar, T. F. Single and multi-functional coating strategies for enhancing the biocompatibility and tissue integration of blood-contacting medical implants. *Biomaterials* **2020**, *258*, No. 120291.
- (114) Primc, G. Recent Advances in Surface Activation of Polytetrafluoroethylene (PTFE) by Gaseous Plasma Treatments. *Polymers* **2020**, *12* (10), 2295.
- (115) Fitriani, S. W.; Ikeda, S.; Tani, M.; Yajima, H.; Furuta, H.; Hatta, A. Physics, Hydrophilization of polytetrafluoroethylene using an atmospheric-pressure plasma of argon gas with water–ethanol vapor. *Mater. Chem.* **2022**, *282*, No. 125974.
- (116) Ayalin, A. A. A.; Go, B. M. S.; Reyes, G. E. S.; Tumolva, T. Characterization of TAPE-Gelatin as a Potential Bioadhesive. *Key Eng. Mater.* **2020**, *833*, 189–193.
- (117) Rajabi, N.; Kharaziha, M.; Emadi, R.; Zarrabi, A.; Mokhtari, H.; Salehi, S. An adhesive and injectable nanocomposite hydrogel of thiolated gelatin/gelatin methacrylate/Laponite as a potential surgical sealant. *J. Colloid Interface Sci.* **2020**, *564*, 155–169.
- (118) Xing, Y.; Gu, Y.; Guo, L.; Guo, J.; Xu, Z.; Xiao, Y.; Fang, Z.; Wang, C.; Feng, Z. G.; Wang, Z. Gelatin coating promotes in situ endothelialization of electrospun polycaprolactone vascular grafts. *J. Biomater. Sci. Polym. Ed.* **2021**, *32* (9), 1161–1181.
- (119) Kopeć, K.; Wojasiński, M.; Eichler, M.; Genç, H.; Friedrich, R. P.; Stein, R.; Singh, R.; Alexiou, C.; Hlawaty, H.; Ciach, T.; Cicha, I. Polydopamine and gelatin coating for rapid endothelialization of vascular scaffolds. *Biomater. Adv.* **2022**, *134*, No. 112544.
- (120) Picco, C. J.; Dominguez-Robles, J.; Utomo, E.; Paredes, A. J.; Volpe-Zanutto, F.; Malinova, D.; Donnelly, R. F.; Larraneta, E. 3D-printed implantable devices with biodegradable rate-controlling membrane for sustained delivery of hydrophobic drugs. *Drug Delivery* **2022**, *29* (1), 1038–1048.
- (121) Laracuenta, M. L.; Yu, M. H.; McHugh, K. J. Zero-order drug delivery: State of the art and future prospects. *J. Controlled Release* **2020**, *327*, 834–856.
- (122) Bil, M.; Kijenska-Gawronska, E.; Glodkowska-Mrowka, E.; Manda-Handzlik, A.; Mrowka, P. Design and in vitro evaluation of electrospun shape memory polyurethanes for self-fitting tissue engineering grafts and drug delivery systems. *Mater. Sci. Eng. C Mater. Biol. Appl.* **2020**, *110*, No. 110675.
- (123) Makvandi, P.; Josic, U.; Delfi, M.; Pinelli, F.; Jahed, V.; Kaya, E.; Ashrafzadeh, M.; Zarepour, A.; Rossi, F.; Zarrabi, A.; Agarwal, T.; Zare, E. N.; Ghomi, M.; Kumar Maiti, T.; Breschi, L.; Tay, F. R. Drug Delivery (Nano)Platforms for Oral and Dental Applications: Tissue Regeneration, Infection Control, and Cancer Management. *Adv. Sci.* **2021**, *8* (8), No. 2004014.
- (124) Douafer, H.; Andrieu, V.; Brunel, J. M. Scope and limitations on aerosol drug delivery for the treatment of infectious respiratory diseases. *J. Controlled Release* **2020**, *325*, 276–292.
- (125) Sumi, C. D.; Heffernan, A. J.; Lipman, J.; Roberts, J. A.; Sime, F. B. What antibiotic exposures are required to suppress the emergence of resistance for Gram-negative bacteria? A systematic review. *Clin. Pharmacokinet.* **2019**, *58*, 1407–1443.
- (126) Jumbe, N.; Louie, A.; Leary, R.; Liu, W.; Deziel, M. R.; Tam, V. H.; Bachhawat, R.; Freeman, C.; Kahn, J. B.; Bush, K.; Dudley, M. N.; Miller, M. H.; Drusano, G. L. Application of a mathematical model to prevent in vivo amplification of antibiotic-resistant bacterial populations during therapy. *J. Clin. Invest.* **2003**, *112* (2), 275–285.
- (127) Hauser, S.; Jung, F.; Pietzsch, J. Human endothelial cell models in biomaterial research. *Trends Biotechnol.* **2017**, *35* (3), 265–277.
- (128) Kinstlinger, I. S.; Calderon, G. A.; Royse, M. K.; Means, A. K.; Grigoryan, B.; Miller, J. S. Perfusion and endothelialization of engineered tissues with patterned vascular networks. *Nat. Protoc.* **2021**, *16* (6), 3089–3113.
- (129) Rahmati, M.; Mills, D. K.; Urbanska, A. M.; Saeb, M. R.; Venugopal, J. R.; Ramakrishna, S.; Mozafari, M. J. Electrospinning for tissue engineering applications. *Prog. Mater. Sci.* **2021**, *117*, No. 100721.